СТЕНДОВЫЕ ДОКЛАДЫ
POSTERS

В. Г. САФИН, А. А. СОЛОВЬЕВ

Санкт-Петербургский государственный электротехнический университет "ЛЭТИ"

АНАЛИЗ ВНЕПОЛОСНЫХ КОЛЕБАНИЙ МЕТОДОМ АМПЛИТУДНЫХ ХАРАКТЕРИСТИК

Abstract. The necessary and sufficient conditions of employment of amplitude characteristics method for out band distortions analysis are formulated. The algorithm for significant dilating of this method application field is described. The iterative spectrum analysis method of non-linear systems to some periodic inputs is described also. It is proved that Picard iterations are special case of proposed method.

Нелинейные процессы, происходящие в радиочастотных трактах (РЧТ) при усилении сигналов с медленно меняющейся амплитудой, являются основной причиной появления нелинейных искажений огибающей и возникновения дополнительных спектральных составляющих, лежащих вблизи спектра полезного сигнала и называемых внеполосными.

Одним из наиболее эффективных методов анализа спектрального состава выходного сигнала РЧТ при периодическом изменении амплитуды входного воздействия является метод амплитудных характеристик, давно [1] и успешно [2, 3] используемый при изучении отмеченных явлений в безынерционных РЧТ. При этом под амплитудной характеристикой понимается зависимость амплитуды Y_n каждой из N гармоник ($0 \le n \le N$) выходного отклика $y(t)$ от амплитуды X входного воздействия $x(t) = X\cos(\omega t + \varphi)$, где ω и φ – его частота и начальная фаза. Обычно амплитудные характеристики задаются в виде степенного полинома

$$Y_n = \sum_{m=n}^{N} A_{nm} X^m \qquad (1)$$

Сам метод базируется на том, что, если X является T-периодической функцией времени, то есть $X(t) = X(t+T)$, то подстановка $X(t)$ в (1) и последующее разложение Y_n в ряд Фурье позволяют найти гармонический состав $Y_n(t)$ и тем самым определить любую из комбинационных составляющих в спектре выходного сигнала.

В общем случае, РЧТ являются не только нелинейными, но и инерционными устройствами, поэтому коэффициенты полинома (1) оказываются комплексными. Тогда

$$\dot{Y}_n = \dot{A}_{n0}\left(\dot{X}\right)^n + \dot{A}_{n1}\left(\dot{X}\right)^n \left|\dot{X}\right|^2 + \ldots = \sum_{k=0}^{\mathrm{K}} \dot{A}_{nk}\left(\dot{X}\right)^n \left|\dot{X}\right|^{2k}, \qquad (2)$$

где $\dot{X}$ – комплексная амплитуда входного сигнала, К – максимальный номер учитываемой гармоники, * - знак комплексного сопряжения, $\dot{Y}_n$ – комплексная амплитуда n-й гармоники выходного отклика (тока или напряжения в любой точке схемы, например, в нагрузке).

Соотношение (2) может быть получено только в том случае, когда исследуемый РЧТ отвечает требованиям диссипа-

тивности и конвергентности, а функционал, описывающий связь между входным и выходным сигналами, – непрерывен. Использование метода амплитудных характеристик для исследования инерционных РЧТ возможно только при выполнении определенных ограничений, накладываемых на полосу частот, занимаемую входным сигналом, или длительность переходных процессов в РЧТ.

Определению условий применимости данного метода для анализа нелинейных искажений (амплитуд комбинационных составляющих) в нелинейных инерционных радиотрактах, разработке алгоритма анализа при невыполнении этих условий и созданию метода ускоренного расчета самих амплитудных характеристик и посвящена настоящая работа.

Для решения поставленных задач представим рассматриваемое устройство в виде обобщенной нелинейной модели (ОНМ) [2] рис.1, описываемой следующей системой дифференциальных уравнений:

$$\mathbf{e}(t) = \mathbf{z}(p)\,\mathbf{i}(t) + \mathbf{u}(t), \qquad (3)$$

где $\mathbf{e}(t) = [e_1(t),...,e_D(t)]^{\mathrm{T}}$, $\mathbf{i}(t) = [i_1(t),...,i_D(t)]^{\mathrm{T}}$,

$\mathbf{u}(t) = [u_1(t), u_2(t),..., u_D(t)]^{\mathrm{T}}$ – матрицы столбцы, соответственно, ЭДС входного воздействия, пересчитанной в каждый из D контуров, токов через резистивные нелинейные двухполюсники и напряжений на них; $\mathbf{z}(p)$- квадратная матрица сопротивлений размерностью $D \times D$; т – знак транспонирования; $p = d/dt$ – оператор дифференцирования; $i_k(t) = \psi_k(u_k(t))$, ($k = 1,2,...,D$) – известная вольтамперная характеристика k-го нелинейного двухполюсника.

Возможность и методы представления реальных РЧТ в виде ОНМ рассмотрены в [2].

Подадим на входные зажимы такого РЧТ сигнал с периодически изменяющейся с частотой F амплитудой и первоначально допустим, что последняя изменяется настолько медленно, что комплексные амплитуды токов и напряжений в схеме успевают отслеживать это изменение. Тогда, комплексная амплитуда любой из гармоник тока в каждом из контуров рис.1 может быть разложена в ряд Фурье и представлена в виде $\dot{I}_{qm}(t) = \sum_{r=-R}^{R} \dot{I}_{qmr}\, e^{j2\pi Frt}$, где $\dot{I}_{qmr}$ – комплексная амплитуда комбинационной составляющей тока в q-м контуре на частоте $m\omega + 2\pi Fr$; R – определяет число комбинационных составляющих, учитываемых в спектре каждой из гармоник токов в любом из D контуров. Все $\dot{I}_{qmr}$ могут быть найдены либо с помощью преобразования Фурье, либо с использованием аналитических соотношений. Так для случаев амплитудно-модулированного, либо двухтонового входных сигналов соответствующие выражения для расчета $\dot{I}_{qmr}$ при известных $\dot{A}_{nk}$ получены в [3] стр. 284. Подстановка найденных значений $\dot{I}_{qmr}$ в (3) должна обращать его в тождество.

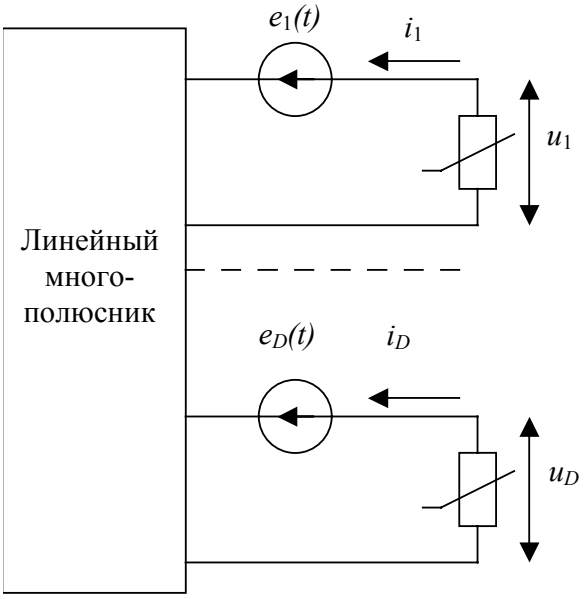

Рис. 1

Для того чтобы комбинационные составляющие оставались неизменными и при больших значениях F, элементы

матрицы $\mathbf{Z}(p)$ при $|r| \le R$ должны обладать следующими свойствами:

$$\left| z_{qk}\left[j(m\omega + 2\pi Fr)\right] \right| \equiv z_{qk}(jm\omega) \neq f(F), \quad (4)$$

$$\arg z_{qk}[j\omega] = a + b\omega. \quad (5)$$

При этом вовсе не обязательно, чтобы модули z_{qk} в спектрах отдельных гармоник (при различных m) были бы одинаковыми. Однако в этом случае на максимальное значение F должно быть наложено очевидное ограничение: спектры гармоник не должны пересекаться, т. е. $4\pi F_{\max} R < \omega$. Наличие одинаковой крутизны фазочастотной характеристики элементов z_{qk} вне зависимости от того, в области какой гармоники она рассматривается, эквивалентно просто появлению соответствующего фазового сдвига у огибающей входного сигнала $X(t)$.

Таким образом, сформулированные условия говорят о том, что коэффициенты, входящие в систему уравнений (3), не зависят от F. Следовательно, не будет зависеть от F и решение этой системы, в том числе и комплексные амплитуды комбинационных составляющих.

Описанные требования обычно выполняются в широкополосных РЧТ. Исключение составляют устройства, в которых условия (4) и (5) не удается выполнить в области постоянной составляющей, из-за противоречивых требований, предъявляемых к номиналам разделительных и блокировочных элементов. Решение задачи спектрального анализа в этом случае для упрощения дальнейшего изложения рассмотрим на примере РЧТ, ОНМ которого содержит всего один нелинейный элемент. Поведение такого устройства описывается скалярным уравнением

$$e(t) = z(p)\, i(t) + u(t), \quad (6)$$

где $i(t) = \Psi[u(t)]$. Допустим также, что производная $d\psi(u)/du = g(u)$ существует. Далее положим, что все $z(m\omega + 2\pi Fr)$ удовлетворяют условиям (4) и (5) кроме $z(2\pi Fh) = z_h = z(0) + \Delta z_h$ и каждую из комбинационных составляющих тока будем определять как $\dot{I}_{mr} = \dot{I}'_{mr} + \Delta\dot{I}_{mr}$, где $\dot{I}'_{mr}$ - комплексная амплитуда комбинационной составляющей тока на частоте $m\omega + 2\pi Fr$ при выполнении условий применимости метода амплитудных характеристик, а

$$\Delta\dot{I}_{mr} = \frac{\partial \dot{I}_{mr}}{\partial z_h}\Delta z_h + \frac{1}{2!}\frac{\partial^2 \dot{I}_{mr}}{(\partial z_h)^2}\Delta z_h{}^2 + \ldots$$

Поскольку $|\Delta z_h| << z(0)$ в последнем выражении целесообразно ограничиться только первым членом ряда.

Можно показать [4], что значения производных $\partial\dot{I}_{mr}/\partial z_h$ могут быть найдены из решения системы уравнений

$$\frac{\partial \dot{I}_{mr}}{\partial z_h} = \sum_{n=-N}^{N}\sum_{p=-R}^{R} z_{np}\frac{\partial \dot{I}_{np}}{\partial z_h}\dot{G}_{m-n,r-p} - \dot{I}_{0h}\dot{G}_{m,r-h}, \quad (7)$$

где $\dot{G}_{m-n,r-p}$ - комплексная амплитуда комбинационной составляющей с частотой $(m-n)\omega + 2\pi F(r-p)$ мгновенной проводимости нелинейного элемента $g(u)$.

При этом определение $\dot{G}_{m-n,r-p}$ не вызывает сложности, поскольку мгновенная проводимость $g(u)$ вычисляется при $\Delta z_h = 0$, т. е. когда известно решение уравнения (6), полученное с помощью метода амплитудных характеристик.

Рассмотренный метод уточнения комплексных амплитуд комбинационных составляющих может быть легко распространен и на устройства, описываемые ОНМ общего вида с той лишь разницей, что число уравнений, входящих в систему, увеличится в D раз и будет равно $D[N]$.

В заключение остановимся на методе определения коэффициентов полинома (2), требующем расчета гармонического состава выходного отклика при различных амплитудах входного сигнала $x(t)$. Одним из наиболее эффективных для решения поставленной задачи является итерационный метод, предложенный в [5]. Его особенности поясним на примере анализа устройств, описываемых уравнением (6).

Предположим, что на итерации с номером l получено решение $u_l(t)$ и $i_l(t) = \psi[u_l(t)]$, лишь приближенно удовлетворяющее (6). Потребуем, чтобы на следующей $(l+1)$-й итерации $u_{l+1}(t) = u_l(t) + \Delta u_l(t)$ и $i_{l+1}(t) = i_l(t) +$, будучи подставленными в (6), обратим его в тождество. Выполнив описанную операцию, несложно получить:

$$z(p)[g_l(t)u_{l+1}(t)] + u_{l+1}(t) = \\ = e(t) - z(p)\{\psi_l(t) - g_l(t)u_l(t)\}, \qquad (8)$$

где $g_l(t)$ - дифференциальная проводимость нелинейного элемента, определенная на l-й итерации.

Решение уравнения (8) удобно выполнить в частотной области. При этом дифференциальное уравнение преобразуется в систему линейных уравнений, размерность которой определяется числом учитываемых гармоник. Численные эксперименты, проведенные в [5], показали, что итерационный процесс сходится достаточно быстро даже в том случае, когда учитывается только постоянная составляющая проводимости $g_l(t)$ равная G_{l0}. В этом случае пропадает необходимость в решении системы уравнений, а соотношение (8) преобразуется к виду

$$[1 + G_{l0}z(p)]u_{l+1}(t) = \\ = e(t) - z(p)\{\psi_l(t) - G_{l0}(t)u_l(t)\}. \qquad (9)$$

Если в уравнении (9) вычисляемое на каждой итерации G_{l0} заменить проводимостью нелинейного элемента в выбранной рабочей точке, т.е. при отсутствии входного сигнала, то получим известную итерационную формулу Пикара [2]. Соотношение (9) легко обобщается и на устройства, представимые ОНМ общего вида. Однако, в этом случае, необходимо будет решать систему из D линейных уравнений.

Описанный итерационный процесс оказывается наиболее эффективным, если расчет амплитудных характеристик начинать с минимальных значений амплитуды входного сигнала, а в качестве первого приближения при каждой новой амплитуде брать решение, полученное при предыдущей.

По найденным таким образом значениям u_k и i_k $(k = 1,2,...,D)$ нетрудно определить сигнал на выходе РЧТ, а его разложение в ряд Фурье – поставить в однозначное соответствие каждому значению X любую из комплексных амплитуд выходного отклика. Аппроксимация полученных таким образом наборов $\dot{X}$ и $\dot{Y}_n$ $(0 \le n \le N)$ степенным полиномом позволяет найти $\dot{A}_{nk}$, входящие в (2). При этом может быть построен не только интерполяционный полином Лагранжа, но и получено среднеквадратическое приближение, либо приближение по Чебышеву.

Литература

1. Бруевич А.Н., Евтянов С.И. Аппроксимация характеристик и спектры при гармоническом воздействии. М.: Сов.радио, 1965.- 343 с.

2. Алексеев О.В., Асович П.Л., Соловьев А.А. Спектральные методы анализа нелинейных радиоустройств с помощью ЭВМ. М.: Радио и связь, 1985.- 152 с.

3. Проектирование радиопередающих устройств с применением ЭВМ. Под ред. Алексеева О.В.. М.: Радио и связь. 1985.- 366 с.

4. Сафин В.Г., Соловьев А.А. Особенности использования метода амплитудных характеристик для спектрального анализа процессов в инерционных нелинейных радиоустройствах // Известия вузов России. Радиоэлектроника, 2000. Вып.2.

5. Сафин В.Г., Соловьев А.А. Итерационные методы спектрального анализа Т-периодического режима в нелинейных радиоустройствах // Известия вузов России. Радиоэлектроника, 2000. Вып.1.

D. J. BEM, T. W. WIĘCKOWSKI

Wrocław University of Technology, Institute of Telecommunication and Acoustics. *Wybrzeże Wyspiańskiego 27, 50-370 Wrocław, POLAND*

EXAMINATION OF THE INFLUENCE OF TRANSMITTER DEVICES ONTO THE ENVIRONMENT.

The introduction into the environment of any objects and in particular ones generating an electromagnetic field requires a number of problems to be resolved in the area of electromagnetic compatibility. In case of radio or television broadcast stations this process starts with the assignment of the frequencies and ends with resolving problems of transmission disturbances and the resistance to the influence of external electromagnetic sources. This article presents a direct examination method for objects surrounding a high power transmission station. The methods have been verified experimentally in practice during the rebuilding of one of the Polish high power (1MW) radio transmission stations operating at a frequency of 225 kHz.

1. Introduction

Any object introduced into the environment shall have the least possible impact onto that environment, whilst itself it shall also resist external influences. This problem is especially significant when the given object is to generate a very powerful electromagnetic field. Starting at the design stage, it shall be evaluated how this object will affect other objects within its surrounding area. This impact in many cases can be evaluated using mathematical methods, however at an environment with many objects present and where they are interconnected through complex networks such mathematical methods fail. For situations like that, the only solution is to measure directly the various objects resistance to external electromagnetic fields, and based on the results of such evaluation determine if the newly planned object can be introduced into that environment or not.

An example of the said situation was the planned building of the Radio Transmission Center near Solec Kujawski for the 1st Program of "Polskie Radio" - transmitting at a frequency of 225 kHz using two quarter-wave antennas supplied with 1 MW of power. This project required several electromagnetic compatibility problems to be resolved, one of them being the determination of the influence onto a unique Radio-astronomy Center located at Piwnice near Toruń (Fig. 1). This Radio-astronomy Center equipped with unique apparatus connected through a complex networks was located within a distance of 21,6 km from the planned transmitting antenna. As one can imagine implementing pure mathematical methods here was impossible.

After the Radio Transmission Center at the Solec Kujawski area is built, the electromagnetic field level at the 225 kHz frequency range shall rise.

Practically every electrical and electronics device shall resist at least an electromagnetic field level with a strength of 3 V/m. One shall take into account however, that in case of the Radio-astronomy Center, which receives very week signals from outer space, an electromagnetic field at 3 V/m could disturb the operations of various sensitive systems installed there. In order to evaluate the resistance of the installations of this Center to electromagnetic fields, it has been decided to perform direct measurements. This method consists of creating the required electromagnetic field (at a level according to standards) within the area where the tested object is located. In the example above, it has been decided to create a local electromagnetic field within the area of the Radio-astronomy Center, with a strength equivalent to that which would be created by the planned Radio

Transmission Center located near Solec Kujawski.

2. Measurements methodology

Measurement of the objects (the installations of the Radio-astronomy Center at Piwnice near Toruń equipped with a 40 meter-high reflector antenna) resistance to electromagnetic radiation, using a direct method consisting of creating within the tested area (the area of the Radio-Astronomy Center) an electromagnetic field with a strength according to the standards. For this evaluation, the electromagnetic field value within the measurement area has been determined based on calculations. This is the value of the field strength that will be created by a quarter-wave antenna supplied with 1 MW of power, who's characteristic has been presented in Fig. 2 and which is to be located at the Radio Transmission Center near Solec Kujawski.

Taking into account that the transmitter creates a vertically polarized wave, our first approximation assumed the radio telescope antenna is a straight 40 meter-high vertical wire.

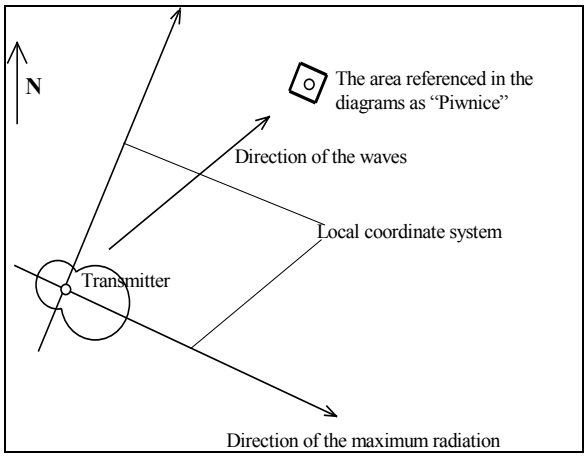

Fig. 1. Location/placement sketch for the electrical field calculations in the vicinity of the radio telescope at Piwnice near Toruń

A computer program has been used for calculating the electromagnetic field strength in the Piwnice area and thus at the Radio-astronomy Center. This computer program uses the moment method for its calculations and it has performed the following calculations:

- calculations assuming that the radio telescope is not present,
- assuming that the radio telescope is present and grounded,
- assuming that the radio telescope is present and not grounded.

The example calculation results are presented in fig. 3. The diagrams present the isolines of the electrical field strength (RMS values) at 2 km x 2 km squares. The wire simulating the presence of the radio telescope has been placed in the center of the coordinate system.

The calculations showed that the electromagnetic field strength within the area of the Radio-astronomy Center will not exceed 400 mV/m. Considering this, in order to evaluate the resistance of the installations of the Radio-astronomy Center to such disturbances, it has been decided to create an electromagnetic field with a strength of 400 mV/m within the evaluated area.

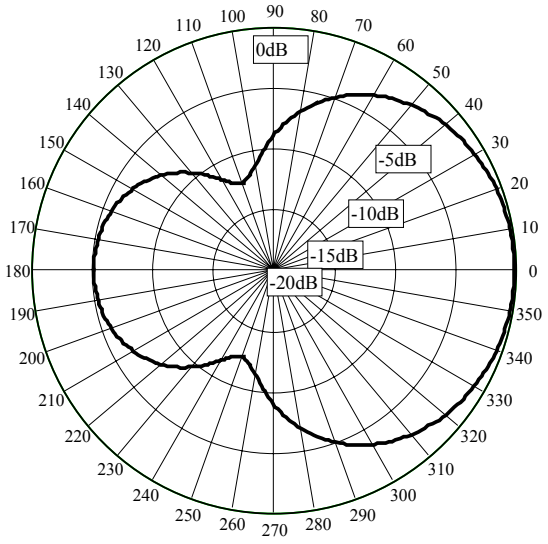

Fig. 2. Optimal antenna transmitting characteristic plot for the transmitting antenna of the Broadcast Center near Solec Kujawski

The high frequency signal that will create this field shall be amplitude modulated with the depth of modulation at 80 %. Such modulation factor is recommended in many standards – also the international ones. Another problem is the frequency of the test signal - a test frequency of 225 kHz can not be used, as the transmission at this frequency would cause a disturbance of the radio pro-

gram emitted from another radio station at Raszyn near Warsaw.

Considering the above another frequency has been chosen as close as possible to 225 kHz. This frequency was 234 kHz.

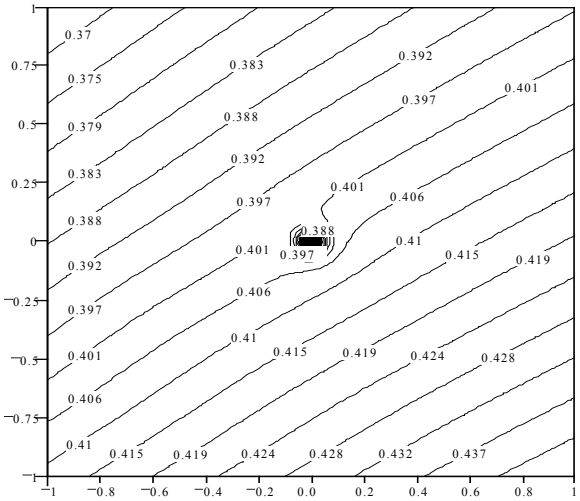

Fig.3. Electric field intensity distribution at the "Piwnice" area assuming that the radio telescope is grounded.

Creating an electromagnetic field with a strength of 400 mV/m and at a frequency of 234 kHz on such a large area as the Radio-astronomy Center, requires not only a high power transmitter but also an antenna capable of radiating such power. In order to simulate most realistically the electromagnetic field that will be present at the Radio-astronomy Center after the Broadcast Center has been built in the Solec Kujawski area, it has been decided to use an single-pole antenna with a ground relative feed. The amount of power radiated by the test antenna does not depend just on the size of the transmitter, but on the matching of its output impedance to the input impedance of the antenna. In order to achieve an input resistance of the antenna similar to that of the transmitter output (50 Ω) an antenna with a height of approximately 333-m is needed. A somewhat smaller antenna can also be used, however an antenna matching circuit or a compensating coil has to be connected between the transmitter and antenna in order to match them together. Unfortunately a solution with any antenna matching circuit or compensating coil cause losses. Since we only had available a linear amplifier (transmitter) with a power of 100 W it was of vital importance to properly match the antenna. An antenna has been made out of copper wire, which has been extended to a height of 333-m using a balloon (Fig. 4).

Fig. 4. Transmitter with linear antenna which has been extended to a height of 333-m using a balloon

An important step in the measurement procedure of the object's susceptibility to electromagnetic fields is the measurement of the electromagnetic field strength distribution within the evaluated space area. A selective voltmeter with a frame antenna is used for measurements of those values. The calibration has been performed for the vertical electrical component of the electromagnetic field. This component will be present within the area of the Radio-astronomy Center after the broadcast center is built. A frame antenna has been chosen as a probe for the electromagnetic field because of two reasons: First, the frame antenna as compared to a linear antenna is less sensitive to other objects within its surrounding. Its input impedance and effective height do not change that much. Second, in reference to distance the changes of the vertical electrical component correspond to the horizontal component (H_φ) of the magnetic field, to which the frame antenna reacts.

After performing all of the necessary calculations, it has been shown that having a transmitter (linear amplifier) with an output

power of 100 W, the required field test level value can be achieved from a distance of about 80 m. The tested installation at the Radio-astronomy Center consists of a reflector antenna and a data handling center, both at a distance of about 240 m apart. It is obvious that with the above setup it is not possible to expose the entire area to an electromagnetic field of at least 400 mV/m from a single point. Considering this, it has been decided to choose two places for installing the test transmitting antennas. On of those places is at a distance of about 70 m from the radio telescope antenna and the other is within a distance of about 70 m from the data handling Center. The measurements for the entire installations' resistance to electromagnetic radiation have been performed twice for both locations of the transmitting antennas.

A significant step of the procedure evaluating the resistance to electromagnetic radiation is the evaluation (measurement) of the object reaction to the electromagnetic field. It is commonly agreed, that the measured parameters and measurement procedures are proposed by the user or the manufacturer of the given object or installation. This user is also the one deciding if he accepts or not the reaction of the tested object or installations. In case of the Radio-astronomy center, a user of that center proposed the tests for evaluating the resistance to electromagnetic disturbances. He also was the one evaluating if the reactions of the object to the electromagnetic field is acceptable or not.

As a result of the tests, it has been judged that the planned Radio Broadcasting Center at Solec Kujawski will not have any negative impact onto the installations of the Radio-astronomy Center.

The proposed measurement method does not allow for the evaluation of the maximum resistance level to electromagnetic disturbances, i.e. the maximum electromagnetic field strength at which the tested object (installations) reaction is still acceptable to the user. In order to determine the maximum resistance level it would be also necessary to find such a value of the field strength, at which the reaction of the object (installation), is not acceptable to the used. Such test would require however transmission equipment with a much higher output power.

3. Summary

The effectiveness of the proposed method for evaluating the resistance of complex installations of the Radio-astronomy Center has been verified after the Radio Transmission Center at Solec Kujawski has been finally built and put into operation. In order to perform that verification, test measurements of the field strength level have been made at the area of the Radio-Astronomy Center at Piwnice (Fig. 6).

These measurements have shown that the measured field strength values (Table 1) fully matched the previous calculations (Fig. 4). It has also been noted, that the present electromagnetic field does not affect negatively the operation of the Radio-astronomy center devices and installations.

Table I. Field strength values at the Radio-astronomy Center after the erection of the Radio Transmission Center

Measurement point	Field strength	
	dB (μV/m)	V/m
Radio telescope	114,5	0,531
Building "I"	114,5	0,531
Building "II"	114,0	0,501
Driveway	112,0	0,398

The proposed method with just a few small modifications (different amplifier type, other transmitting antenna, and other test frequencies) can be successfully used to evaluate the impact of transmitting devices onto various objects within their surrounding.

References

[2] EN 50082-1, "Electromagnetic compatibility, Generic immunity standard, Part1: Residential, commercial and light industry".

[3] EN 50082-2, "Electromagnetic compatibility, Generic immunity standard, Part2: Industrial environment.

R.J. KATULSKI[1], A. KOSINSKI[2]
J. STEFANSKI[1], R. STUDANSKI[2]
[1]Technical University of Gdansk, PL-80-952 Gdansk, Poland
[2]Naval Academy, PL-81-919 Gdynia, Poland

MEASUREMENTS OF THE ELECTROMAGNETIC INTERFERENCES IN A COMPUTER NETWORK

Abstract: In the paper the electromagnetic interferences analysis due to their influences on the wire local computer network in a ship scenario is presented. First, the functionality form of the designed measurement's network is described. Next, the obtained measurements are discussed. The researches were carried out for the computer network with the RS232C interface type.

1. Introduction

In a modern ship command systems the informatic technology is applied, especially to obtain a real time of decision processes. The informatic structure based on a computer network. The electromagnetic interference signals induced in the wires of the ship computer network, due to another all the ship electric equipment and installations, is a very important problem connected with the electromagnetic compatibility condition of the network. A knowledge of a character and a type of the interference signals is necessary to increase of the operational reliability of the ship command system [1].

2. Measurement's System

The block scheme of the measurement's system, which based on the wires of the computer network, is shown in Fig. 1.

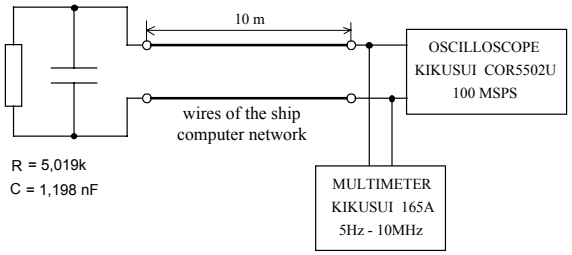

Fig. 1. Block scheme of the measurement's system

For the measurement's procedure the computer network wires are connected with:

- the RC circuit as equivalence of the computer interface input,
- the measurement's equipment, i. e. with the oscilloscope and voltage multimeter.

The RC load measurement's wires was fixed according to recommendation to interface RS232C with 20 kbps transmission rate. The shape of the wires were fixed individual depending on a character of measurement's place.

The interferences signals were defined as voltage time waveforms at output of twisted wires. Each waveform was surrendered to mathematical analysis. The interferences impulses with 50 Hz sine curve waveform background were analysed.

3. Results of the Investigations

The electromagnetic interference were measured in:

- command platform,
- marine power plant,
- along corridor with radio equipment neighbourhood,
- gyro-compass and fan rooms,
- the rudder neighbourhood,
- the windlass neighbourhood.

The obtained results were analysed and presented in graphical forms. The exemplary obtained results are shown in Figs. from 2 to 8, in which the asterisk denote the frequency scale ratios.

The electromagnetic interfernce measured in the command platform are shown in Fig. 2.

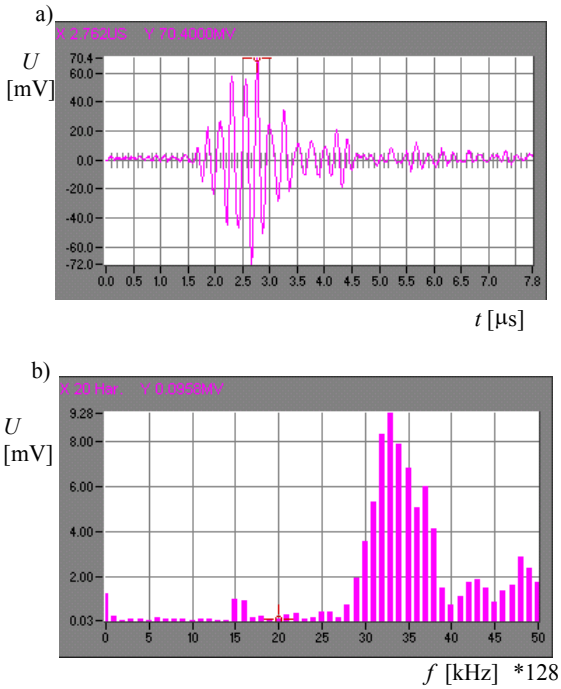

Fig. 2. The electromagnetic interference measured in the command platform:
a) time waveform, b) spectrum form

In this case, the unregular interference is occurred at frequency about 4,2 MHz and occupied 1,7 MHz bandwidth. High level of the interference was descended from the ship radio transmitter.

The interference phenomena along the corridor with radio equipment neighbourhood, with switched HF ship radio transmitter, were carried out too. These exemplary measurement's results were shown in Fig. 3.

The voltage interference signals due to the carrier signal and the harmonics of the radio transmitter are induced in the computer network wires with the 200 mV peak value.

The results of the electromagnetic interferences measurements in the ship power plant are shown in Fig. 4.

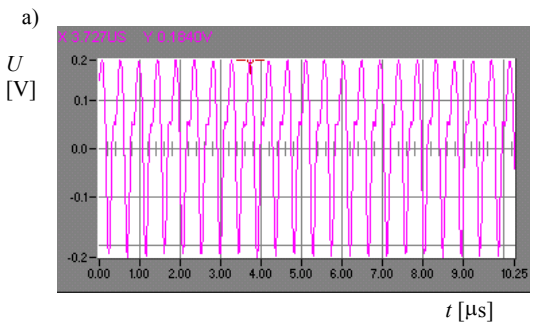

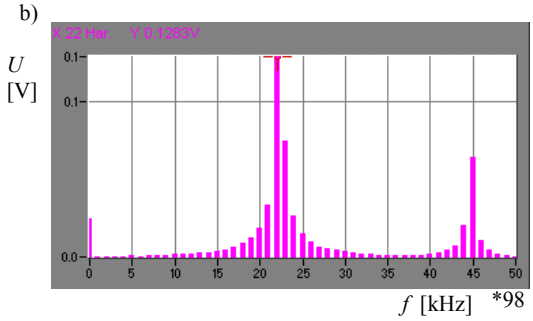

Fig. 3. The electromagnetic interference results measured along the corridor with the radio equipment neighbourhood:
a) time waveform, b) spectrum form

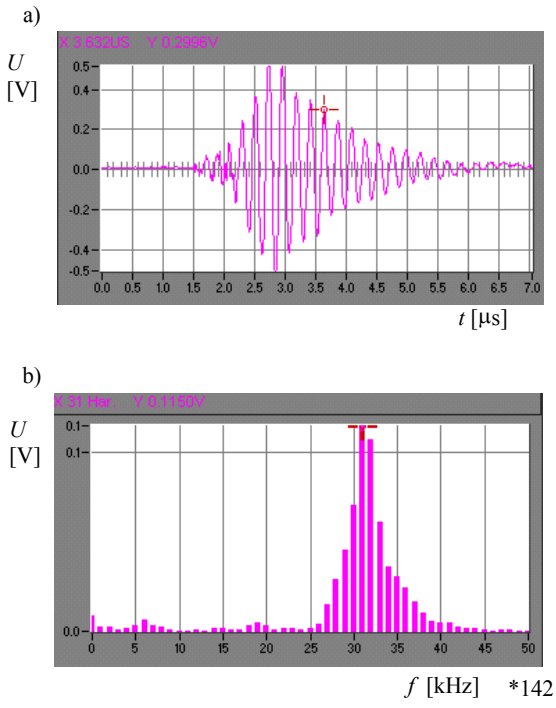

Fig. 4. The electromagnetic interference measured in the ship power plant:
a) time waveform, b) spectrum form

The great value of the unregular impulse were observed, which mid-band frequency was 4,4 MHz, with frequency bandwidth equals 1,8 MHz.

Interference measured in gyro-compass room were shown in Fig. 5.

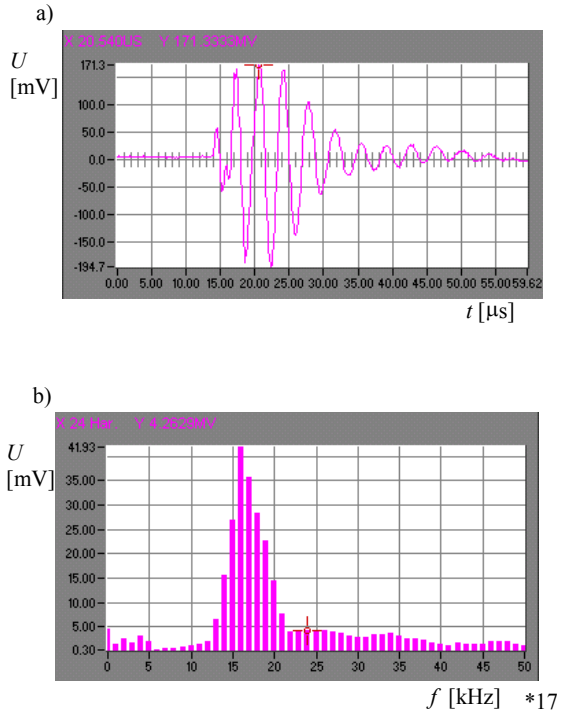

Fig. 5. The electromagnetic interference results measured in gyro-compass room:
a) time waveform, b) spectrum form

There are impulse interference too. The mid-band frequency is 1 MHz, with 170 kHz bandwidth.

In the warship scenario the ship demagnetizer is a source of the interference signals. The interference signals measured at demagnetizer neighbourhood is shown in Fig. 6.

The mid-band frequency of the interference signals is 270 kHz, with 180 kHz bandwidth. Spectrum form of the signal includes low frequency which influenced on transmission quality of the tested computer network, with low transmit rate.

The interference problem at the neighbourhood of rudder is shown in Fig. 7.

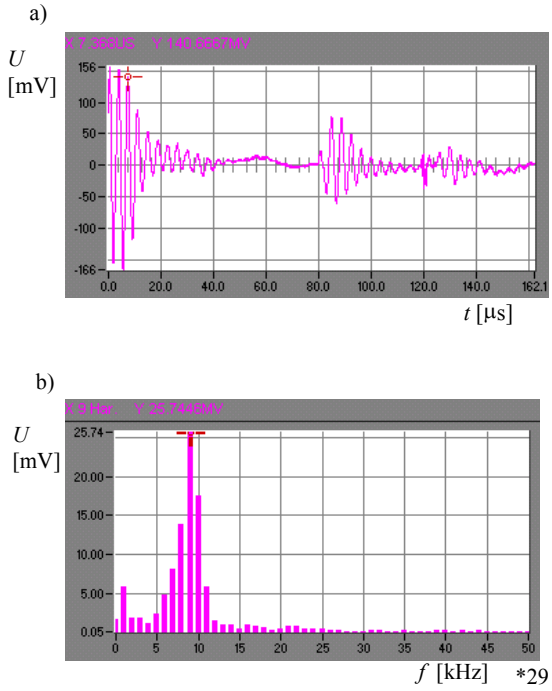

Fig. 6. The measured demagnetizer electromagnetic interference signals:
a) time waveform, b) spectrum form

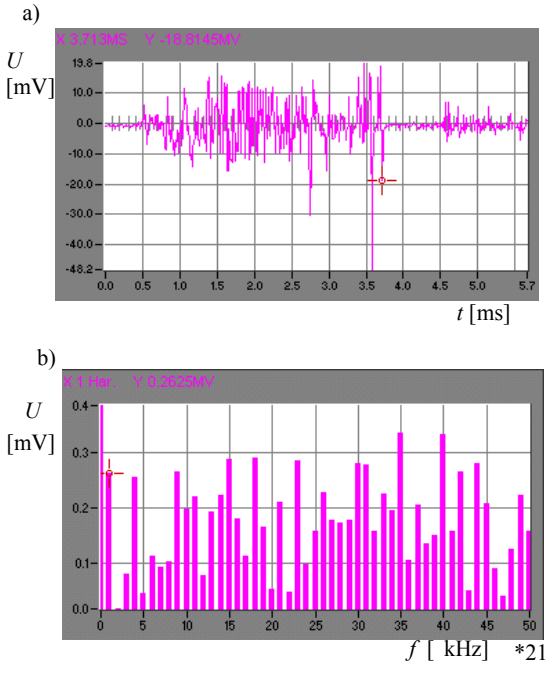

Fig. 7. The measured interference signal at the neighbourhood of rudder:
a) time waveform, b) spectrum form

In the above presented figure we can see so the spectrum of the interference signal

have low frequency components with low power level.

The interference results in the neighbourhood of windlass were shown in Fig. 8.

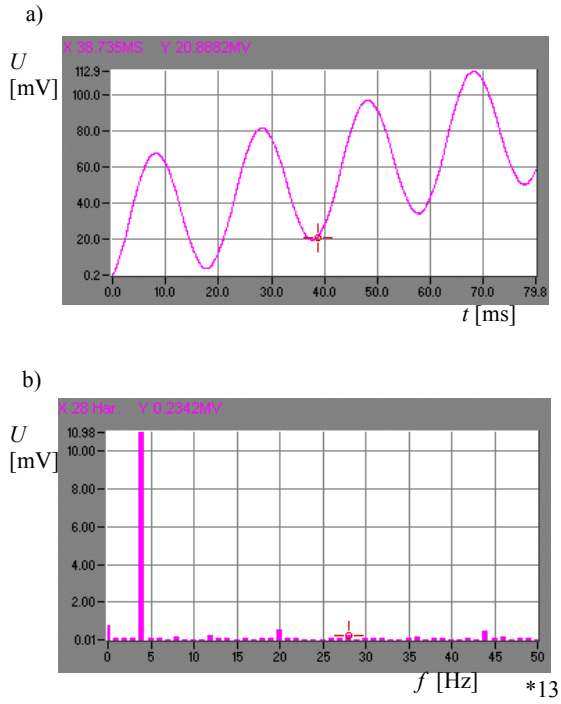

Fig. 8. The electromagnetic interference results measured in the neighbourhood of windlass: *a) time waveform, b) spectrum form*

Presented spectrum graph shows basic component of 50 Hz.

Moreover, on the tested ship the interference from the ship supply system are occurred. The measured peak values were shown in Table I.

Table I: The measured interference signal peak values

Measurement's place	Peak value [mV]
Windlass neighbourhood	9
Fan room	11
Gyro-compass room	13

4. Analysis of the EMI Condition

In attempt to examine an influence of the EM interference (EMI) signals on a ship computer network, the bit error rate (BER) of the tested computer network transmission, for RC232C interface, was measured. The block scheme of the measurement's system is shown in Fig. 9.

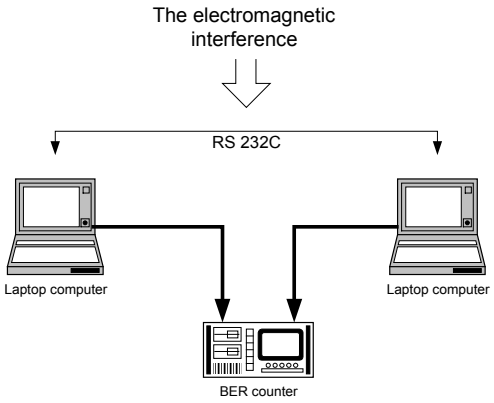

Fig. 9. The block scheme of the BER measurement's system

The data transmission was realised by use two wires form of cable of the computer network, with length about 40 meters, type BASE-T. To eliminate an influence of the EM interference through power supply network in both computers the battery supplies have been applied. The experiments were carried out in the ship power plant.

Generally, electromagnetic interference signals induced in the ship computer network not affected to transmit quality. Errors appeared sporadically.

5. Conclusions

Taking into account above presented measurement's results the following conclusions can be formulated:

- ship computer network should be carefully screen,
- computer network power supply system should be galvanic isolate from ship power supply,
- data transmit rate should be individual tamper with computer network.

Reference

[1] Garus at all, *EMI Analysis in a Warship Computer Network*, Proc. of the Conf. on Military Comm., Zegrze-Poland 2000, pp. 71-74.

BEKTAŞ ÇOLAK[1,2] OSMAN ÇEREZCİ[2] BAHATTIN TÜRETKEN[1]
[1]TÜBİTAK UEKAE, EMC Labratory, Tel:+90 262 6481235
[2]Sakarya University, Dept. of Electric & Electronics

MODELLING THE COAXIAL DOUBLE BRAIDED SCREENS

Abstract. In this paper we tried to obtain the effect of the direct leakage term of the diomand shaped holes to the circuit parameters of the double braided screens for the measurement of the transfer impedance according to the IEC Triaxial test setup. We focused on the direct magnetic coupling mechanism. This information should be used for the optimization of the double braided screens.
Keywords: Screening efficiency, Transfer impedance, Coaxial cable, Double braid, Optimization.

Introduction

The screening effectiveness of the coaxial cable screens measured via several methods. We are dealing here with IEC triaxial short circuited method (Fig.2). The braid structure made by strands of helically interwoven wires and there are diomand shaped holes at the crossing point of the strands.

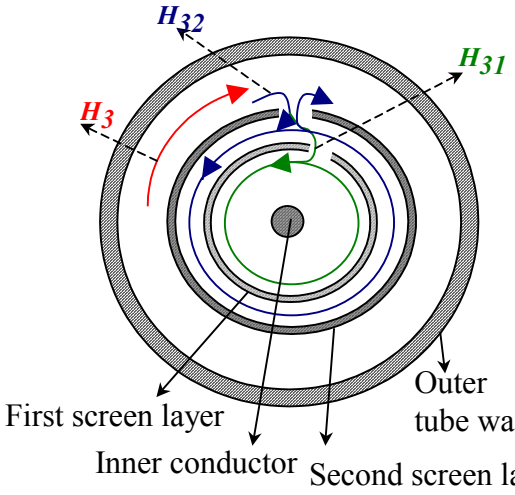

Fig.1. Cross-section of the double screened cable and magnetic leakage from diomand shaped apertures

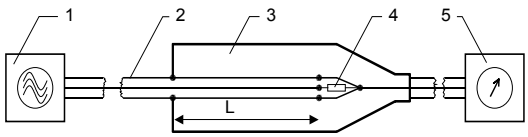

1 – Signal generator, 2 – Coaxial cable under test, 3 – Measuring tube, 4 – Termination load, 5 – Receiver, L – Coupling length
Fig.2. IEC Triaxial Short Circuited Test Method

The electromagnetic energy generated between the outer wall of the measurement tube and the cable screen leaks, from this holes directly (Fig.1). This leakage defined as the hole inductance and effective at higher frequencies. At low frequencies diffusion of the induced currents on the screen is effective. These parameters are measured as the transfer impedance Z_T, and it is a measure of the screening effectiveness of the cable screen and defined as the quotient of the longitudinal voltage measured on the secondary side of the screen to the current in the screen, caused by a primary inducing circuit, related to unit length Fig.3. [10].

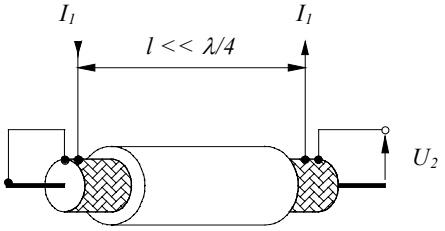

Fig. 3. Definition of transfer impedance

$$Z_T = \frac{U_2}{I_1 \cdot l} \qquad (1)$$

On the other hand, there is another important standardised quantity, the capacitance coupling admittance Y_T, *and it* is defined as the quotient of the current in the screen caused by the capacitive coupling in the secondary circuit to the voltage in the primary circuit related to unit length [10] (Fig.4). But we focused on the Z_T term here.

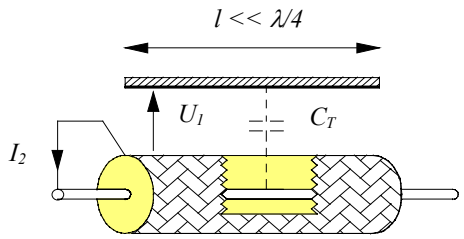

Fig. 4. Definition of coupling admittance

$$Y_T = \frac{I_2}{U_1 \cdot l} = j\omega \cdot C_T \qquad (2)$$

For single braided screens, many authors worked on the calculation of this coupling parameters. The earlier works were done by Kaden [1], and Schelkunoff [2]. The relation between the braid paramers and coupling parameters are given by Vance[3]. Detailed works focused on the braid optimization were done by Homann[4], Tyni[5], Fowler[6] and Halme[7]. For high efficiency of the screening without loosing the flexibility of the coaxial cable, double layers of braided screen are used. Sali has done a work for the triaxial cables as a special case of double braids[11]. Althought many valuable attemps to find the analytical expressions for the coupling parameters there were still big differences between the theory and experiment. Kley[8] tried to remove this differences by semi-emprical model. His work based mainly to [1],[2] and [5]. He modified the formulations by some constants via experiments.

Direct leakage mechanism

In this paper we focused on the direct magnetic coupling mechanism of the diomand shaped holes at braid surface. Ikrath[9] has done an extensive work on the effect of apertures of the coaxial cable screens by assuming them as planar mesh surfaces. Therefore it incluedes the error term. We modified this method for the cylindrical braid surface. Referring to the Fig.5. we can investigate the interaction of the magnetic field lines at each layers. If we consider the real measurement situation, first and second layers are short circuited at both ends. Therefore for initial condition the total disturbing current, I_3, flows from each wires (i) at both braid layers equally.

$$i = \frac{I_3}{n_1 + n_2} \qquad (3)$$

where, n_1 and n_2 are the total wire numbers for first and second layers respectively.

By applying the Ampere law,

$$H_{3r_{22}} = \frac{I_3}{2\pi r_{22}} \qquad (4)$$

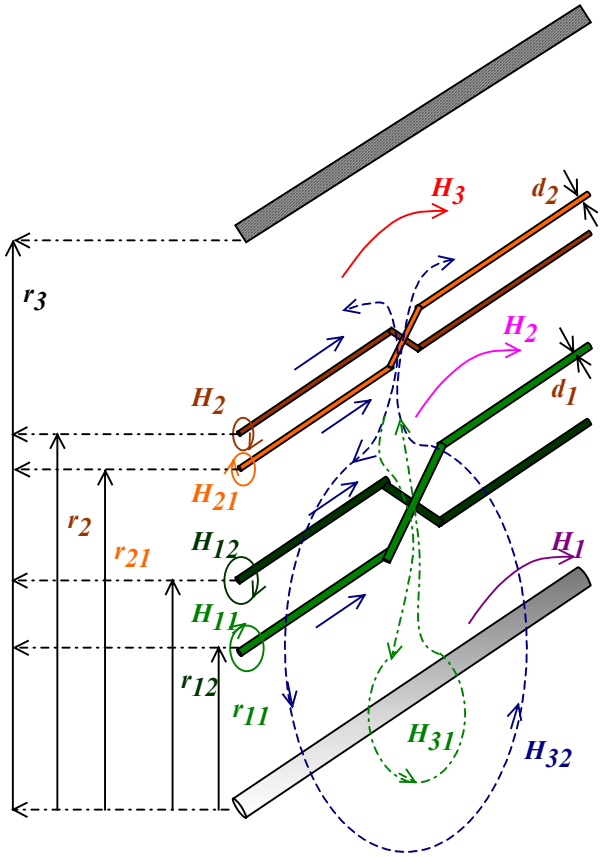

Fig.5. Individual and the leakage magnetic lines at double braided cable screen under test setup The layers from top to dip are; Setup wall, upper braid layer halves, inner braid layer halves and the interior conductor respectively.

Since the braid structure includes diamond shaped apertures, some of the magnetic flux lines penetrate from this apertures through to the interior conductor. The leakage flux in the intermediate section between the both braid layers are related with the surface of the apertures. From the

Induction law, the electromotor force produced by this leakage is;

$$V_{32} = -\frac{\partial \Phi_{32}}{\partial t} \qquad (3)$$

where,

$$\Phi_{32} = -\mu_0 \iint H_{3r_{22}} ds_{32} \qquad (4)$$

The mutual inductance of the apertures at second layer is;

$$M_{32} = \frac{\upsilon_2 \Phi_{32}}{I_{32}} \qquad (5)$$

where, υ_2 is the number of apertures at unit lenght of the second layer braided screen.

In order to find the mutual inductance of the aperture firstly we have to obtain the normal component of the H field to the aperture surface. The normal component of surface magnetic field to the hole surface is calculated by superposition of each single wire to the hole center. As a first step we consider only the effect of the nearest wires to the hole center. (Fig.6).

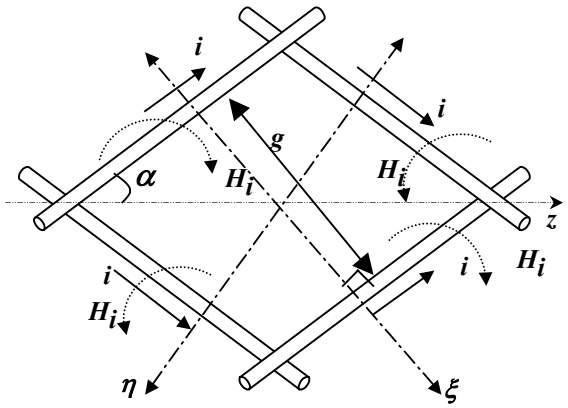

Fig.6. Magnetic fields in the diomand shaped hole

Since the H field is normal to the current direction, we have to define new axis as η and ξ normal to the each wire direction. At the center along the z axis, each H fields cancel each other. By the way the magnetic field lines enter to the inside of the interior layer from the upper triangular part of the z axis and go out from the lover part. Since the H fields must close around themselves a rotation occurs around the z axis. Therefore an e.m.f. produced per unit lenght of the z axis[9]. If we adds the effects of the all wires to this aperture we obtain the total magnetic fields normal to the aperture surface.

$$H_{\eta,\xi} = \sum_{i=1}^{M/4} \sum_{j=1}^{N} \left[\frac{1}{r_{ij}+\eta} - \frac{1}{r_{ij}-\eta} + \frac{1}{r_{ij}+\xi} - \frac{1}{r_{ij}-\xi} \right] \frac{\cot(\frac{r_{ij}}{2a})}{4\pi} \qquad -g/2 \langle \eta, \xi \langle + g/2 \qquad (6)$$

where r_{ij} is the distance between the aperture center and j.wire of the i.belt and calculated as

$$r_{ij} = (i-1)W + (j-1)d + \frac{W-(N-1)d}{2} \qquad (7)$$

where, d: diameter of each wire, i: index of the belt number and i=1..M/4, j:index of the wire number and j=1..N, M: total belt number at the braided screen, N: total wire number at each belt of braid, W:belt plus aperture width and given at [3] as

$$W = \frac{4\pi a \cos\alpha}{M} \qquad (8)$$

where a is the radius of the braided screen layer. The last *cotan* term of the (6) is added for the curvature of the cylindrical shield. For the cylindrical coordinates transformations from ξ and η to r, θ and z should be taken into account.

In Fig.7 a sample calculation is done in order to show the variation of the H field around the z axis.

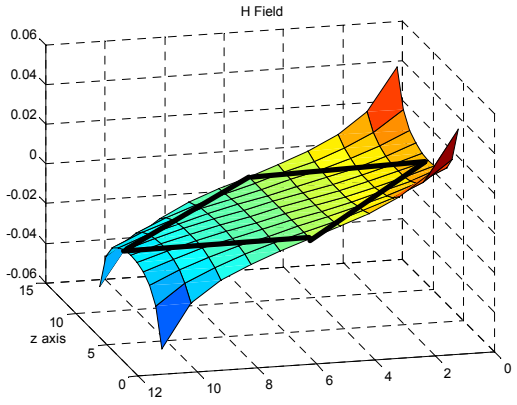

Fig.7. Calculated value of H field. The values out of the border of the diomand shall be omitted.(M = 24, N = 8, d = 0.15 mm, i = 1Amp $\alpha = \pi/6$)

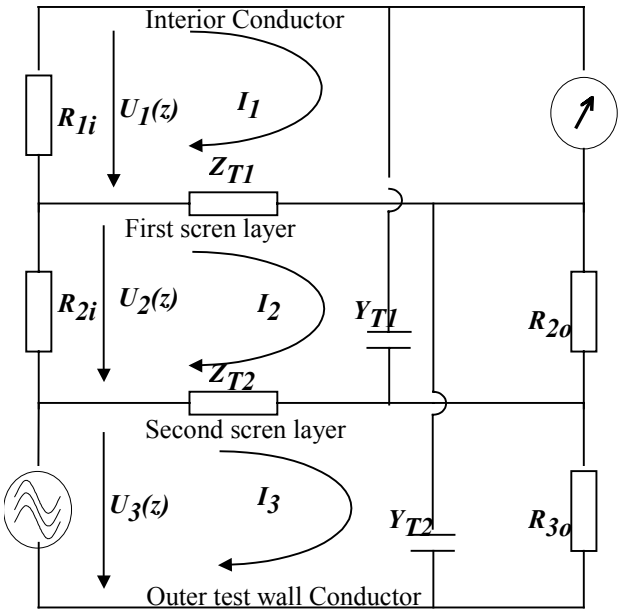

Fig.8. Equivalent Circuit Model of coupling parameters for double braid screened coaxial cable

Now we are able to calculate the mutual inductance of the aperture via (5) by putting the (6) at (4). Tha care should be taken also for the integration surface of the aperture. It should be taken over the upper or the lower triangular part. The same steps can be done also for the first layer. The calculation of the Z_T and the C_T can be found at [7] with emprical modifications of the formulations. We are not going to repeat them. After finding the coupling parameters of each layer, Fig.8 can be used for the transmission line equations. For the test conditions R_{30}, R_{2i}, R_{20} is short circuited and R_{i1} is equal to the characterictic impedance of the cable.

The optimization process includes the porposing coupling [8] and try to balance the imaginer component of the high frequency term of the Z_T as if the magnetic field lines coupled to the interior conductor. Between the first layer and the interior conductor the final fields should be considered at this layer for optimization. The H_{32} and H_{21} are the leakage fields from the screen and the H_{11} is at inverse direction with these fields. H_{11} brings the braid inductance via porposing effect. This interaction should be calculated at the outer surface of the interior conductor.

Conclusion

The direct magnetic leakage term of the diomand shaped apertures of the coaxial braided screen are modified for the real geometric conditions of the cylindrical shield structure as if including the curvature and the limited number of the wires. In order to obtain the circuit parameters of the braid one should be care of the terminating resistors. As a further work, measured values and the merit of the accuracy of the direct leakage calculations will be compared.

References

[1]. H. Kaden, Wirbelströme und Schirmwirkung in der Nachrichtentechnik, Berlin, Springer, 1959.

[2] Schelkunoff, S. A. the electromagnetic theory of coaxial transmission lines and cylindrical shields, Bell System Technical Journal. Vol.13 pp.552.579, Oct. 1934.

[3]. E. F. Vance, “Shielding Effectiveness of Braided Shields”, IEEE Transaction on Electromagnetic Compability, Vol 17,No 2,May 1997,pp 71-77

[4]. E. Homann, "Geschirmte Kabel mit optimalen geflectschirmen", Nachrichtentechishe Zeitschrift, Vol.21, No.3, pp-155-161, 1968

[5]. M. Tyni, The transfer impedance of coaxial cables with braided outer conductor. 3rd Wroclaw Symposium on EMC,1976, pp.410-418.

[6]. E. P. Fowler, "Superscreened Cables", The Radio and Electronic Engineer, Vol. 49, No. I, pp. 38-44, Jan. 1979.

[7]. Thomas Kley, "Optimierte Kabelschirme- Theorie und Messung", Ph.D. dissertation, Swiss Fed. Inst. Tech., Zurich, 1991.

[8]. P.J. Madle, "Contact Resistance And Porpoising Effects in Braid Shielded Cables", Conference Proceedings on IEEE EMC, 1980, pp 206-210.

[9]. Lothar O. Hoeft, Joseph S. Hofstra, "Experimental Evidence for Porpoising Coupling and Optimization in Braided Cables", Conference Proceedings on IEEE EMC, 1998, pp 505-509.

[10].IEC-Standard 61196-1 (1995-05), 12. Screening effectiveness

[11]. S. Sali, "Screening Efficiency of Triaxial Cables with Optimum Braided Shields", IEEE Transaction on Electromagnetic Compatibility, Vol 32, No 2, May 1990, pp 125-136.

BAHATTIN TÜRETKEN, ALI İHSAN YÜREKLI

TÜBİTAK – UEKAE EMC Laboratory, Gebze 41470 Kocaeli – TURKEY. Tel:+90-262-648 10 00, Fax:+90-262-648 11 00
e-mail: bahattin@uekae.tubitak.gov.tr

MEASURING EMC ANTENNA FACTORS: COMPARISON OF ANTENNA CALIBRATION METHODS

Determining the antenna factor (AF) is a major step in making field strength measurements accurately for EMC compliance. There are well-established antenna calibration methods [1-3] to calculate these antenna factors in Open Area Test Sites (OATS). However, alternative methods utilizing different test sites, like Gigahertz Transverse Electromagnetic (GTEM) Cell, are also brought forth in recent years. In this study, antenna factor measurement and calculation with standard and alternative methods are performed. The reliability of alternative methods are discussed. Antenna factors of an UK NPL calibrated, small-size log periodic antenna are first determined on TÜBİTAK – UEKAE premises using standard methodology. The log-periodic antenna is then placed at the center of the test volume of a GTEM 1750 cell. With the fact that field strength produced in the GTEM is proportional to the signal applied to the input and using the definition of antenna factor, the antenna factor is calculated by measuring the GTEM input signal and antenna output voltage Since the accuracy of this method is dependent on the size and positioning of the antenna, antenna factor measurements are carried out for 4 different positions inside GTEM and resultant data are compared with original (NPL) and user (TÜBİTAK-UEKAE) data. Additional work is performed to determine transmit antenna factor of the same antenna, using the reciprocity property of the GTEM cell.Upto this point, this study covers only a log-periodic antenna of small size. The same procedure iscarried out for a large size log-periodic antenna, as well.

1. Introduction

Antennas and sensors play an important role in EMC compliance testing. The accuracy of calibration of these devices determines the accuracy of radiated-emissions (RE) and radiated-susceptibility (RS) test results.

Antenna calibration is the process of determining the numerical relationship, within an overall stated uncertainty, between the observed output of a measurement system and value, based on standart sources, of the physical quality being measured.

The antenna factor (AF) is a ratio of measured E or H-field strength to the induced voltage delivered at the output of he antenna. AF must be highly accurate and the equipment used for measurement must be traceable to a national standart.

Some commonly used methods of determining antenna factors are given below

- Rod Antennas (9kHz-30MHz)
  SAE ARP 958 Rev D[1]
  ANSI C63.5-1998 (ECSM)[2]
- Biconical Antennas (30-300 MHz)
  ANSI C63.5-1998 (SSM)[3]
- Log_Per Antennas (300-1000MHz)
  ANSI C63.5-1998 (SSM)
- Horn Antennas (1-40 GHz)
  SAE ARP 958 Rev D

In this paper, we have obtained antenna factors of two different antennas from 30 MHz to 1000 MHz in Open Area Test Site

[1]The Engineering Society For Advancing Mobility Land Sea Air and Space –Aerospace Recommended Practice

[2]American National Standart for Electromagnetic Compatibility- Radiated Emission Measurements in Electromagnetic Interference (EMI) Control-Calibration of Antennas (9kHz to 40 GHz)_Equivalent Capacitance Substitution Method

[3]American National Standart for Electromagnetic Compatibility- Radiated Emission Measurements in Electromagnetic Interference (EMI) Control-Calibration of Antennas (9kHz to 40 GHz)_Standart Site Method

and the GHz Transverse Electromagnetic Cell (GTEM).

2. A method of determining AF (OATS)

We have used ANSI C63.5-1998 (SSM) Method in OATS. The SSM (based solely on horizontally polarized measurements) provides antenna factor measurements from 30 MHz to 1000 MHz. The measurement distance are 3m and 10 m, transmit antenna heights are 1m and 2m, and receive antenna search heights are from 1 m to 4 m. The methods shall be used for horizontal polarization on a standard antenna calibration site.

2.1. Description of Method

The SSM requires three insertion loss measurements under identical geometries using three identical antennas taken in pairs, as shown fig.1

$$AF_1 + AF_2 = A_1 + 20\log(f_{MHz}) - 48.92 + E_{Dmax} \quad (1)$$

$$AF_1 + AF_3 = A_2 + 20\log(f_{MHz}) - 48.92 + E_{Dmax} \quad (2)$$

$$AF_2 + AF_3 = A_3 + 20\log(f_{MHz}) - 48.92 + E_{dmax} \quad (3)$$

(All equaitons in dB)

where

$A_{1,2,3}$: Measured insertion losses(dB)

E_{Dmax}: is the maximum received field at seperation distance R from the tranmitting antenna

AF_1, AF_2, AF_2,: are the antenna factors of antennas (dB(1/m))

f_M is the frequency in MHz

Solving equations (1), (2)and (3)

$$AF_1 = 10\log f_M - 24.46 + 1/2[E_{Dmax} + A_1 + A_2 - A_3] \quad (4)$$

$$AF_2 = 10\log f_M - 24.46 + 1/2[E_{Dmax} + A_1 + A_3 - A_2] \quad (5)$$

$$AF_3 = 10\log f_M - 24.46 + 1/2[E_{Dmax} + A_2 + A_3 - A_1] \quad (6)$$

2.2. Measurement Procedures

There are two measurement procedures that may be used to determine insertion loss- *a discrete frequency method* and *a swept frequency method*

We have used *a swept frequency method* based on a computer programme (Fig 1.)

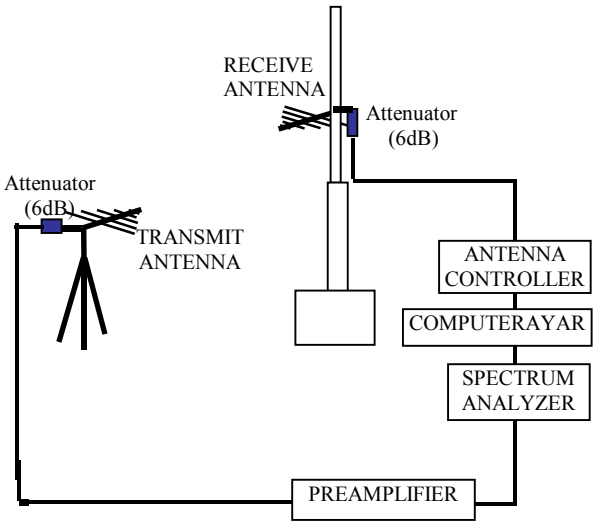

Figure 1. Geometry of antenna calibration setup (OATS)

3. An alternate method of determining AF (GTEM)

The method of calibration an antenna in GTEM is to place the antenna in the center of the test volume, aligned such that the linearly polarized antenna is oriented vertically in the linearly polarized test volume and the floor of the GTEM (see Fig 2)

The field strength in GTEM is,

$$E = \frac{V_i}{h} \quad (7)$$

where:

E: Electric Field Strength, (Volts/meter)

V_i: Input RF Voltage (Volts)

h: Septum Height, (meter)

The definition of antenna factor is:

$$AF = 20\log(\frac{E}{V_0}) \quad (8)$$

where:

AF: Antenna Factor, (m^{-1})

E: Electric Field strength, (Volts/meter)

V_0: Antenna output voltage (Volts)

Combining (7) and (8) gives:

$$AF = 20\log(V_i) - 20\log(V_0) + 20\log(1/h) \quad (9)$$

A small log periodic antenna (Schwarzbeck 9108 –217) was placed in the test volume of GTEM 1750 and calibrated by using Fig 2. Test Setup from 300 MHz t0 1 GHz)

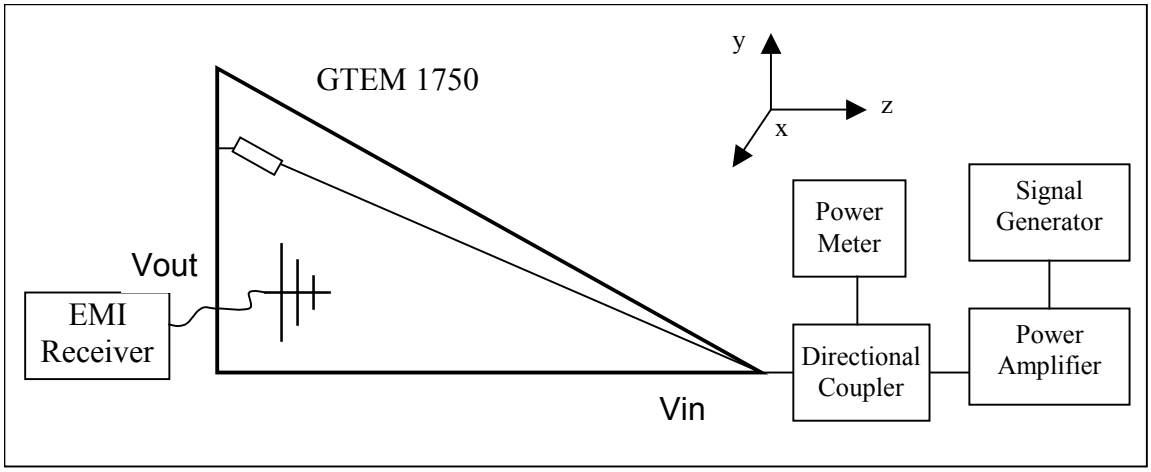

Figure 2. Test Setup for Determining the Antenna Factor in a GTEM cell

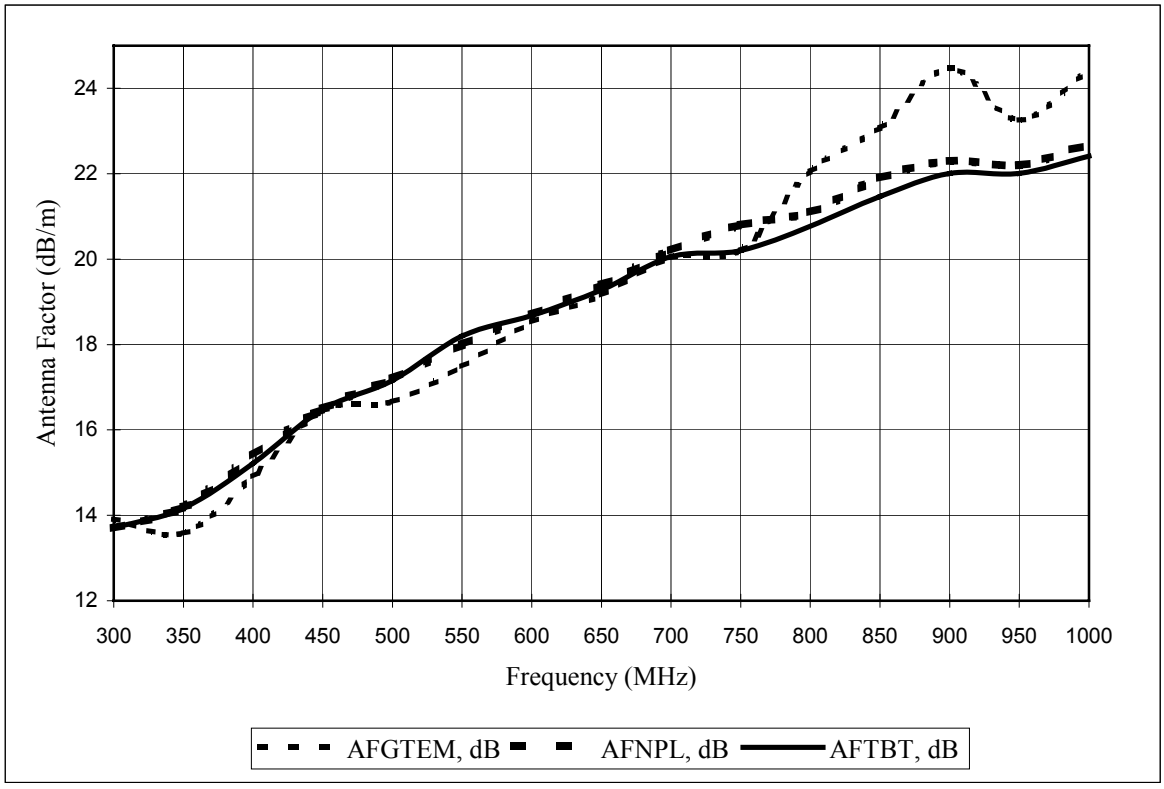

Figure 3. Antenna Factors of Schwarzbeck Log-Peryodik Antenna (s/n:217) (30MHz–300MHz)

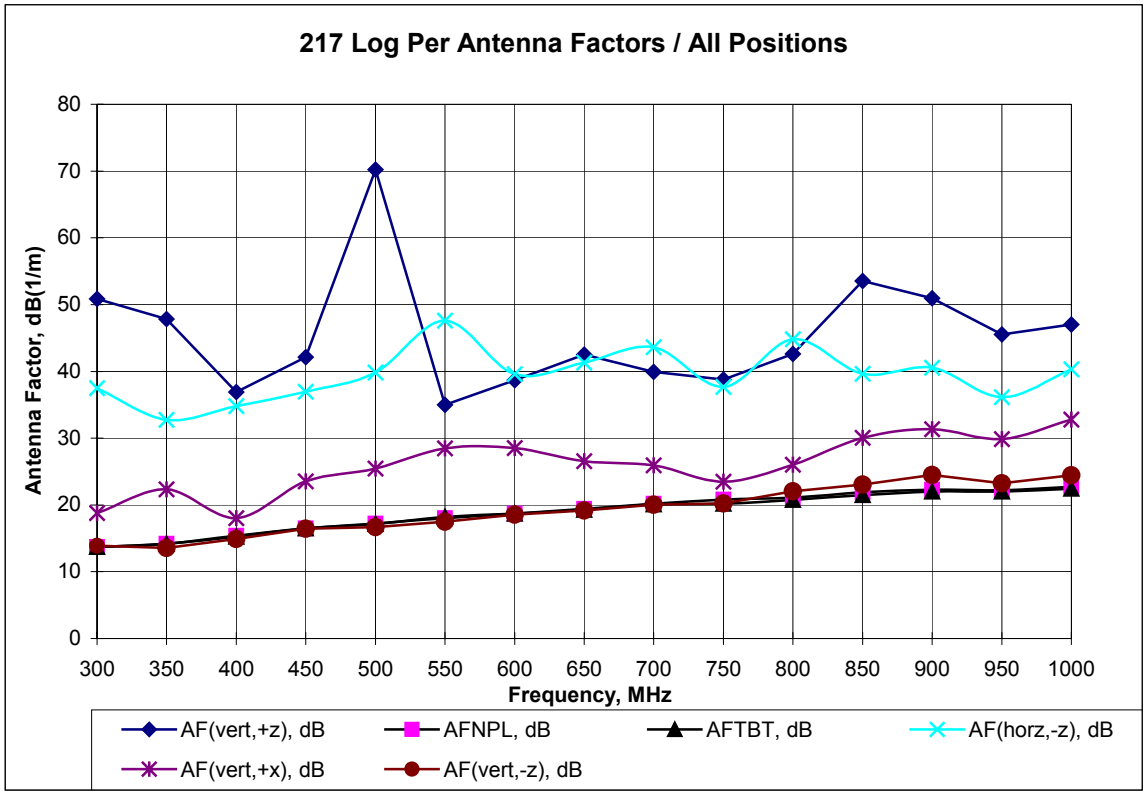

Figure 3. Antenna Factors of Schwarzbeck Log-Periodic Antenna (s/n:217) (30MHz–300MHz) (All Positions)

6. Conclusion

The following general conclusions are peresented

1. A very good agreement between The NPL measurement and TUBITAK-UEKAE OATS measurement have been presented.
2. A new method of determining AF in GTEM has been implemented.
3. The advantages of GTEM for antenna factor determination over traditional EMC measurements are:
   - Ambient signals are not a factor
   - Measurements may be carried out at a convenient location
4. The disadvantage of the GTEM is the limited test volume.
5. The most suitable results was obtained at the (–z) position of the Log.Periodic antenna as vertical polarization
6. Transmit Antenna Factor of Schwarzbeck Log Periodic Antenna (s/n:217) has been obtained in GTEM.

Refences

[1] NSI C63.5-1998 American National Standart for Electromagnetic Compatibility-Radiated Emission Measurements in Electromagnetic Interference (EMI) Control-Calibration of Antennas (9 kHz–40 GHz).

[2] SAE ARP 958 The Engineering Society For Advancing Mobility Land Sea Air and Space, 1999.

[3] Ranaugh E.L., Osburn J.D.M. Measuring EMC Antenna Factors in The GHz Transverse Electromagnetic Cell. IEEE, 1992.

ALI İHSAN YÜREKLI, BAHATTIN TÜRETKEN
TÜBİTAK – UEKAE EMC Laboratory, Gebze 41470 Kocaeli – TURKEY. Tel:+90-262-648 10 00, Fax:+90-262-648 11 00
e-mail: yurekli@uekae.tubitak.gov.tr

RF FIELD MEASUREMENT AND THEORETICAL CALCULATION FOR CELLULAR BASE STATION ANTENNAS

In this study, the radiation characteristics of cellular base station antennas are investigated. As a first step, the total radiation of an array-antenna which is intended to transmit in the GSM 900 MHz band is obtained analytically. The antenna under investigation is an array of four vertical dipoles positioned along the z-axis [1-3] The method is explicit and, once the radiation characteristic of any single dipole has been calculated analytically, the general pattern of the array can then be calculated. Secondly,. measurements are carried out on different points near an actual base station transmitter which is designed to transmit in the 1800MHz range. Final discussion is on the determination of the minimum distance to a BSA in order to comply with international RF safety guidelines.

1. Introduction

Health hazard aspects of exposure to radio frequency (RF) energy radiated by cellular base station antennas (BSA) have been of great concern in recent years. The public interest in the subject triggered scientific research in parallel with the increasing number of BSA which became visible in public areas.

Scientific research on this area can be divided into two major categories: First is the characterization of the RF field generated by the BSA and incident upon the public. Second is the investigation of biological effects of these electromagnetic fields. While the former category is a subject of application of electromagnetic theory, the latter needs biological and medical expertise to reach a conclusion.

Characterization of the RF source is very important since biological effects are mostly dependent on the field strength level, frequency and signal characteristics. Many analytical and numerical techniques have been used to obtain the radiation characteristics of these antennas so far.

2. Analytical solution

Usually the radiation pattern of a single element is relatively wide, and each element provides low values of directivity (gain). In many applications, it is necessary to design antennas with very directive characteristics (very high gains) to meet the demands of long distance communication. This can only be accomplished by increasing the electrical size of the antenna.

One way to enlarge the dimensions of the antenna, without necessarily increasing the size of the individual elements, is to form an assembly of radiating elements in an electrical and geometrical configuration. This new antenna consist of multi elements and is called as “an array”. The total field of the array is determined by the vector addition of the fields radiated by the individual elements.

2.1. Four- Element Array

Base anttennas are formed by using half-wavelength dipole as a collinear array.

The total radiation of this array-antenna is obtained analytically. The antenna under investigation is an array of four vertical dipoles positioned along the z-axis,behind a metallic reflector, as shown in Figure 1.

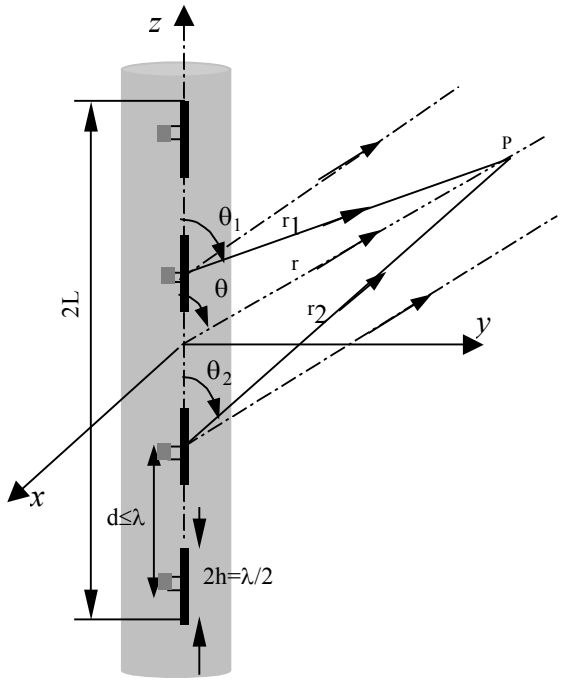

Fig. 1. Schematic view of the studied dipole array antennas

The field at an observation point P can be described as the sum of fields radiated by four dipoles in the presence of the reflector.

$$\vec{E}t = \vec{E}_1 + \vec{E}_2 + \vec{E}_3 + \vec{E}_4 \qquad (1)$$

$$E_t = \mathrm{j}\eta\frac{kI_0 l}{4\pi r} f(\theta) e^{-j\beta r}\Big[1 + \zeta_1 e^{j(\alpha_1 + \beta\,\vec{a}_r \vec{r}_1)} \ldots\ldots \ldots\ldots \underbrace{+\zeta_{\mathrm{i}} e^{j(\alpha_i + \beta\,\vec{a}_i \vec{r}_1)} \ldots + \zeta_{n-1} e^{j(\alpha_{n-1} + \beta\,\vec{a}_i \vec{r}_{n-1})}}_{\text{Array Factor (AF)}}\Big] \qquad (2a)$$

$$\frac{I_i}{I_0} = \zeta_{\mathrm{i}} e^{j\alpha_i} \qquad (2b)$$

$$f(\theta) = \frac{\cos(\frac{\pi}{2}\cos\theta)}{\sin\theta} \qquad 2c)$$

where;

η is the free-space waveimpedance

k is wave number

l is dipole length ($l = \lambda/2$ for half-wave dipole)

$f(\theta)$ is radiation pattern factor of unit antenna (half-wave dipole)

r is distance between antenna and point P

I_0 is electric current on unit antenna

ζ_{i} is electric current on i-th antenna

$\vec{a}_r$ is unit vector on r-direction in spherical coordinates

$\vec{r}_i$ is position vector i-th antenna.

Total field has been illustrated so that the far-zone field of uniform four-element array of identical elements is equal to the product of the field of single element, at a selected reference point (usually the origin), and the array factor of that array. That is

$$\mathrm{E} = [\mathrm{E}_{(\text{single element})}] \times \times [\text{Array factor (AF)}] \qquad (3)$$

$$AF = \sum_{n=1}^{N} e^{j(n-1)\psi_z} \qquad (4a)$$

$$\psi_z = \alpha_z + \beta d_z \cos(\theta) \qquad (4b)$$

After some mathematical manipulations (4a) reduces to

$$(AF)_n = \frac{1}{N}\left[\frac{\sin(\frac{N}{2}\psi)}{\sin(\frac{\psi}{2})}\right] \qquad (4c)$$

The total field of four half-wave dipole z-axis have been obtained analitically,

$$E_{tz} = j\eta\frac{I_0}{2\pi r} f(\theta,\phi)\left[\frac{\sin(\frac{N_z}{2}\psi_z)}{N_z \sin(\frac{\psi_z}{2})}\right] e^{-j\beta r} \qquad (4d)$$

The contribution of metallic reflector can be added to equation (4d) by using image theory.

$$E_{tzy} = E_{tz}\left[\frac{\sin(\frac{N_y}{2}\psi_y)}{N_y \sin(\frac{\psi_y}{2})}\right] \qquad (5a)$$

$$\psi_y = \alpha_y + \beta d_y \sin(\theta)\cos(\phi) \qquad (5b)$$

To find the nulls of the array on the z-axis, (4d) are set equal to zero. That is,

$$\theta_{nz} = \cos^{-1}\left[\frac{\lambda}{2\pi d_z}(-\alpha_z \pm \frac{2n_z}{N_z}\pi)\right]$$

$$n_z = 1,2,3...$$

$$n \neq N_z, 2N_z, 3N_z...$$

The maximum values of (4d) occur when

$$\theta_{mz} = \cos^{-1}\left[\frac{\lambda}{2\pi d_z}(-\alpha_z \pm 2m\pi)\right],\ m_z = 0,1,2,3...$$

$$\theta_m = \cos^{-1}\left[\frac{\lambda\alpha_z}{2\pi d_z})\right],\ m = 0$$

The 3-dB point for the array factor (4d) occurs,

$$\theta_{hz} = \cos^{-1}\left[\frac{\lambda}{2\pi d_z}(-\alpha_z \pm \frac{2.782}{N_y}\pi)\right]$$

$$n = 1,2,3...$$

$$n \neq N_z, 2N_z, 3N_z.$$

By the same way to find the nulls, the maximum values and the 3-dB point of the array on the y-axis occur when,

$$\theta_{ny} = \cos^{-1}\left[\frac{\lambda}{2\pi d_y}(-\alpha_y \pm \frac{2n}{N_y}\pi)\right]$$

$$n_y = 1,2,3...$$

$$n \neq N_y, 2N_y, 3N_y...$$

$$\theta_{my} = \cos^{-1}\left[\frac{\lambda}{2\pi d_y}(-\alpha_y \pm 2m\pi)\right],\ m_y = 0,1,2,3...$$

$$\theta_{my} = \cos^{-1}\left[\frac{\lambda\pi\alpha_y}{2\pi d_y})\right],\ m = 0$$

$$\theta_{yh} = \cos^{-1}\left[\frac{\lambda}{2\pi d_y}(-\alpha_y \pm \frac{2.782}{N_y}\pi)\right]$$

$$n_y = 1,2,3...$$

$$n \neq N_y, 2N_y\ 3N_y.$$

In this problem,

$N_z = 4$,

$N_y = 2$,

$\lambda = 0.33\text{m}$,

$$d_z = \frac{\lambda}{2}$$

$$d_y = \frac{\lambda}{4}$$

$$\psi_z = \pi\cos(\theta)$$

$$\psi_y = \pi + \frac{\pi}{4}\sin(\theta)\cos(\phi),$$

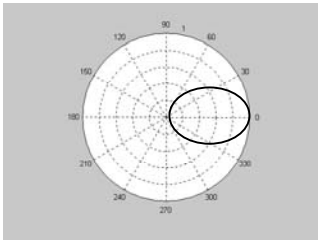

Fig. 2. The radiation pattern of array on the z-axis in the horizontal plane for 900 MHz

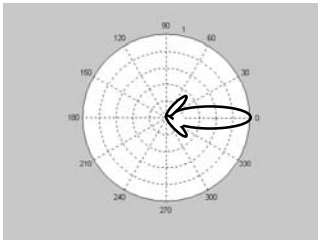

Fig. 3. The radiation pattern of the array on the z-axis in the vertical plane for 900 MHz

3. Measurement

An experimental setup was developed in an Open Area Test Site (OATS), to evaluate the E–field distribution in the far field region of radio base station (RBS) antennas. A commercial RBS antenna (Kathrein 739491) was tested (see Fig 4) at 1800 MHz.

Fig 4. Photo of experimental set-up on the OATS

The antenna was mounted on a vertical scanning system. An isotropic E-field probe, Holaday Industries HI-4456 (30MHz-18GHz), was used to measure the E-field at

different angles 6 m away from the RBS antenna.(see Fig 5.).

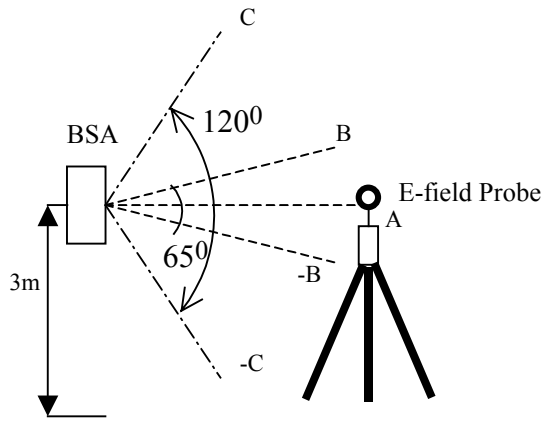

Fig 5. Measurements points

We have obtained similar results in our measurements compared to the manufacturer's data. The ground effect was neglected in the measurements.

4. Conclusion

- An analytical solution of the BSA (900 MHz) was presented.
- The far field produced by the BSA Kathrein 739491 (1800MHz) was measured.
- When 120 Watts power was applied to the antenna, the safety guideline recommendation given by ICNIRP was passed for a distance of less than 6.1 meters from the antenna for 1800 MHz.

References

[1] Altman Z, Karwowski A, Wong M.F, Wiart J, Gattoufi L., "Dosimetric Analysis of Base Station Antennas via Simulation and Measurements" EMC 2000 International Wroclaw Symposium on Electromagnetic Compatibility 210-244 June 27-30, 2000 Wroclaw, Poland

[2] Balanis C.A., "Antenna Theory Analaysis and Design" 2nd ed. John Wiley &Sons, Inc.1997

[3]Cristoforetti L. et al., " E- Field Evaluation in The Near and Fresnel Regions of Dipoles Array Antennas". Millenium International Workshop on Biological Effects of Electromagnetic Fields October 17-20, 2000, Heraklion, Crete, Greece

A. P. NICKOLAENKO

Usikov Institute for Radio-physics and Electronics of the National Academy of Sciences of the Ukraine

NUMERICAL MODEL FOR THE NATURAL ELF RADIO NOISE

Abstract. We describe the results of numerical modeling of the natural ELF radio noise in the Earth-ionosphere cavity. A signal simulated for the vertical electric field component in the frequency range of the Schumann resonances has many feature pertinent to real records. In particular, it is exhibits the natural stabilization of spectral estimates similar to those observed experimentally.

Natural radio noise in the ELF frequency band (from 3 Hz to 3 kHz) is generated by electromagnetic radiation from the global thunderstorm activity. Individual lightning strokes occur at random, hence a statistical approach must used for the modeling of the noise background. We describe the vertical component of the ELF radio noise in the time domain as a following succession of random electromagnetic pulses:

$$E(t) = \sum_{k=-\infty}^{\infty} A_k \cdot e_k(t - t_k) \qquad (1)$$

Here A_k is the amplitude of the k-th random pulse, t_k is the arrival time of the random pulse, $e_k(t)$ is the k-th pulse waveform. Summation of pulses is formally held from $-\infty$ to $+\infty$ having in mind that in accordance with the causality principle the waveform $e_k(t)$ equals to zero when the argument is negative $t < t_k$.

Elementary waveform of the arriving pulse is found from the following equation (*Nickolaenko and Rabinowicz*, 2000):

$$E(x,t)=\mathrm{Re}\left\{A\cdot E_A\cdot\vartheta^{-B}\left[R_{-1}+(R_0-1)B+\left(\frac{R_1}{\vartheta}-1\right)B(B+1)+\sum_{n=1}^{\infty}\frac{B(B+1)^2\vartheta^n}{(n-B)(n+1)}P_n(x)\right]\right\} \quad (2)$$

where the amplitude of the field $E_A=\dfrac{M_C}{2\pi h a^2\varepsilon}$, M_C is the current moment of the k-th lightning stroke, h is the height of the Earth-ionosphere cavity, where the waves propagate, a is the Earth-radius, and ε is the dielectric constant of vacuum. We suppose that the complex propagation constant of the radio wave is a linear function of frequency: $\nu(f)=Af+B$, parameter $\vartheta=\exp\left(i\dfrac{t}{A}\right)$, $x=\cos\theta$, θ is the distance from the observer to the k-th stroke, the R-functions are:

$$R_0(\vartheta,x)=\frac{1}{\left(1-2x\vartheta+\vartheta^2\right)^{1/2}},$$

$$R_{-1}(\vartheta,x)=\frac{1-x\vartheta}{\left(1-2x\vartheta+\vartheta^2\right)^{3/2}}-1, \quad \text{and}$$

$$R_1(\vartheta,x)=\ln\frac{\vartheta-x+\sqrt{1-2x\vartheta+\vartheta^2}}{1-x}$$

(*Nicolaenko and Rabinowicz*, 2000).

Since the attenuation of electromagnetic waves is small at ELF, the pulse rate in (1) equals to that of overall vertical strokes taking place worldwide (up to 100 events per second). Individual pulses substantially overlap and form a continuos SR background noise. An important assumption is the mutual independence of all model parameters: pulse amplitudes, their arrival times, and coordinates of the sources.

The random variables are generated with the standard modern software supplied with a personal computer. The basic procedure is the obtaining of random numbers uniformly distributed on the [0; 1] segment. We generate and use such a succession after its renormalization to generate the quasi-random set of the source distances. We had postulated that distance from the observer to the strokes is uniformly distributed around median value of 10 Mm within the 5 Mm gap: it is found with equal probability between 7.5 and 12.5 Mm. These is a realistic distance distribution for the observer places in the Central Europe and the sources situated in the South America (Brasilia) or in the East Asia (Indonesia).

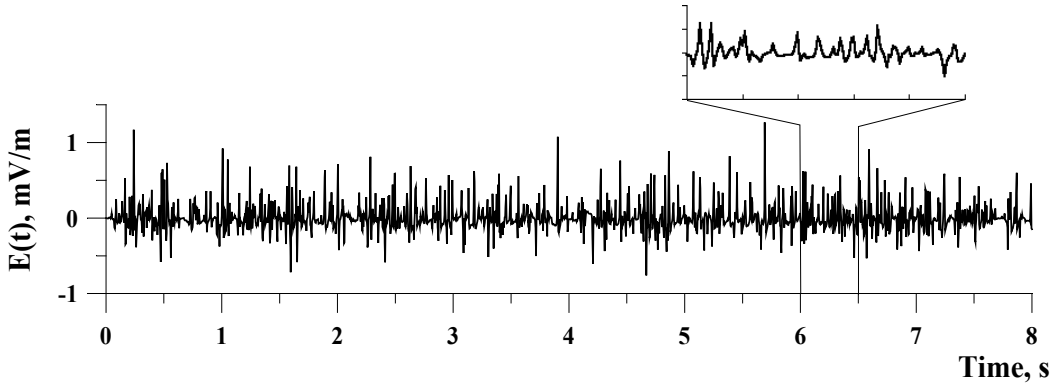

Fig. 1. ELF signal composed as a random Poisson pulses with the rate of 50 eve/s. D ∈[5, 10 Mm], and amplitudes have the Gaussian amplitude distribution. Sampling frequency is 204.8 Hz.

Since the lightning discharges are the Poisson succession, we construct a process with the exponential probability distribution of the waiting times between the pulses $w(\Delta t)=Le^{-L\Delta t}$. Deviates y are obtained from the variable x uniformly distributed in [0; 1] interval by introducing a formula $y=-\log(x)$. The pulse rate L is 50 events per second. The normal random numbers for the source amplitudes are obtained from x by the Box-Muller method. The median current moment of the source $\langle M_C\rangle = 6\times10^7\ A\times m$, and its standard deviation $\sigma_M = 16\times10^7\ A\times m$.

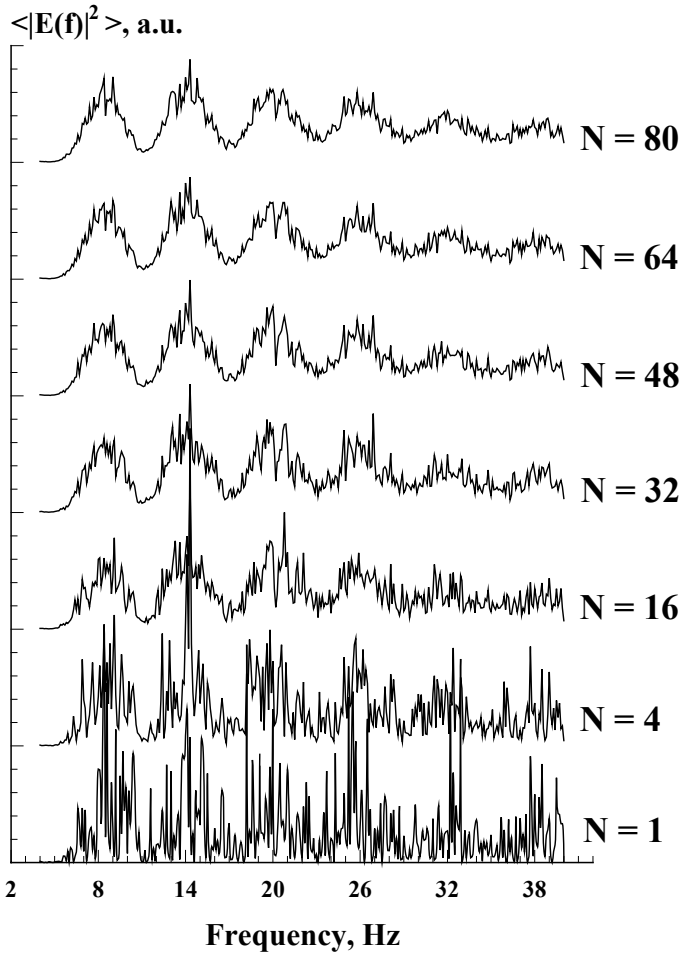

Fig. 2. The model of natural stabilization of spectral estimates of the SR.

We simulated the vertical electric field component with the sampling frequency of 204.8 Hz. A fragment of this 'record' is shown in Fig. 1. Time in seconds is shown along the abscissa on linear scale. The vertical electric field is shown along the ordinate in *mV/m*. We do not include into the model a man-made interference and suppose that the receiver has an infinite band width. Figure demonstrates that the background ELF noise is a composition of pulses. At extended time scales, the signal looks like a continuous line, see the waveform between 6 and 6.5 s in the insert. Rapid variations of the signals become depressed when a band-pass filtering is used.

The model SR signal is applied for demonstrations of natural stabilization of the Schumann resonance spectral estimates. The processing of the data set was made in the following way. Pieces of the record 10 s long (sets of 2048 real numbers) were processed with the standard FFT algorithm. The individual power spectra were accumulated (averaged) as this is done in the real data acquisition systems [*Belyaev et al*., 1999]. The 'current' results of spectral processing are presented in Fig. 2.

The lowest irregular curve in Fig. 2 represents individual power spectrum obtained for the first 10 sec of the record. Stabilizing results of further averaging are shown by the curves shifted vertically. Numbers N to the right of the curves depict the quantity of individual spectra included in the averaging procedure (each of these corresponds to the record 10 sec long). One may see that the procedure of the data accumulation effectively smoothes the resulting spectra, and the Schumann resonance peaks become clearly seen after a few minutes accumulation.

Spectra in Fig. 2 display that the time of the data accumulation must exceed approximately 5 minutes (N > 32). The spectral stabilization and necessary duration were stud-

ied experimentally long ago. Now, are able to construct a model ELF signal pertaining this characteristic properties.

The inevitable long duration is not obvious beforehand. We had used the rate of 50 events per second in the above simulations. This means that about three thousand events are averaged every minute, and this number seams to be great. The experiment and the above model demonstrate that this is not so. A more detailed inspection shows that simultaneous variability appropriate to the sources in time, space in the amplitudes increases the necessary ensemble by a factor of ten. Spectra of Fig. 2 demonstrate also that the fine structure does not completely vanish even when the observation time exceeds the 10 minute interval.

To conclude the report we must note that the above ELF radio signal could be used for testing and tuning the experimental equipment as well as for interpretations of observations.

References

1. Belyaev, G.G., A.Yu. Schekotov, A.V. Shvets, A.P. Nickolaenko, Schumann resonances observed using Poynting vector spectra, *J. Atmos. Solar-Terr. Phys*., **61**, 751-763, 1999.

2. Nickolaenko, A.P., and L.M. Rabinowicz, Accelerating of the convergence of the time-domain solution for lightning stroke ELF pulses, *Radio-physics and Electronics,* **5**, No.1, 108-112, 2000 (in Russian).

ALEXANDER V. SHVETS

Usikov Institute for Radiophysics and Electronics, National Academy of Sciences of Ukraine

SPATIAL STRUCTURE OF THE AFRICAN WORLD THUNDERSTORM CENTRE DEDUCED FROM DIRECTION FINDING OF VLF ATMOSPHERICS

Abstract. A technique of tomographic reconstruction of the spatial structure of lightning activity is proposed. The technique is based on measurements of azimuthal distributions of atmospherics from different distant receiving stations. An effective algorithm for tomographic reconstruction has been developed to reduce required computational resources. The spatial structure of thunderstorms in Africa has been estimated from results of direction finding of VLF atmospherics performed from board the scientific vessel during March-April, 1991. The results of reconstruction show that stable active areas correspond to the Niger and Congo basins, Madagascar, and coastal part of the Guinea bay.

1. Introduction

Remote global lightning activity observations are considered at present as a promising means for monitoring of global environmental changes [1]. The precise technique for locating lightning discharges provides optical observations from the space, but considerable cost and limited area of viewing from satellites leave us reasons for consideration traditional radio physical methods for lightning observation. LF and VLF atmospherics produced by lightning return strokes are used for lightning location with good precision (of order a few kilometres) within limited areas up to size of a few thousand kilometres [2]. Usually such lightning detection networks operate far from main tropical lightning sources (with some exclusions, see e.g. [3]) and employ rather sophisticated synchronously operating equipment.

In this work we discuss locating African thunderstorms, based upon tomographic reconstruction by results of multi-site direction finding of atmospherics. The technique proposed does not require identification of every atmospheric at each receiving point and in such way simplifies the realisation of observations. The tomographic technique proposed has been developed for the aim of the lightning distribution reconstruction on the base of the so called “pixel” approach and as a

result of modification of the method described in the previous work [4]. As tomographic projections we employ histograms of azimuthal distributions of atmospherics measured from a network of direction finders.

2. Procedure of tomographic reconstruction

A simplified experimental setup for tomographic measurement, shown in Fig. 1, looks like classic triangulation system. Azimuthal distributions of atmospheric are measured at each point of the direction finder network during a certain time period. The histograms of atmospherics arrival directions obtained are considered as different projections for tomographic reconstruction of the surface distribution of lightning discharges.

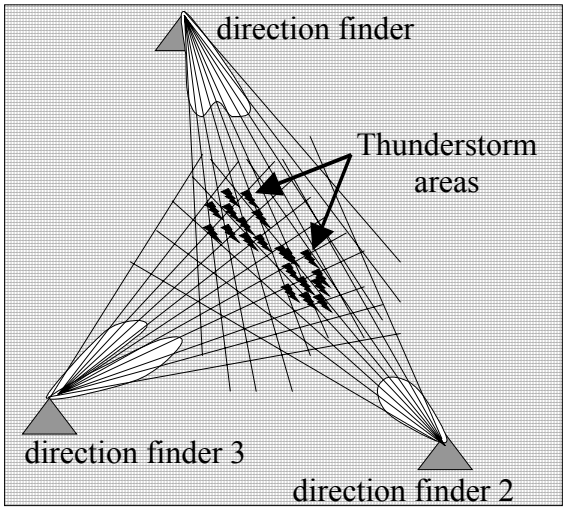

Fig.1

Supposing that the monitored part of the earth surface is represented by a net of ordered discrete points in which we will determine numbers of produced lightning discharges and choosing a finite, small enough, elementary sector size in the azimuthal histograms we can formulate the task of the tomographic reconstruction in the next linear algebraic equation system:

$$S_{ki} = \sum_{j=1}^{M} W_{kij} s_j ; k = 1..K, i = 1..N, j = 1..M \quad (1)$$

where S_{ki} is an a number of atmospherics registered within the i^{th} elementary sector of the histogram measured from the k^{th} receiving point, W_{kij} is a system matrix, determined by geometry of receiving point distribution, s_j is an unknown number of lightning discharges assigned to j^{th} discrete point of the earth surface, K is a number of the receiving points, M is a dimension of the unknown vector $\vec{s}$, N is a number of elementary sectors in the azimuthal histograms. The equation (1) states that the integral number of atmospherics corresponding to the elements of the vector $\vec{s}$ dropping into the i^{th} sector of the k^{th} histogram is equal to i^{th} element of the k^{th} histogram. The elements of the system matrix can take values of 0 or 1. The system matrix W_{kij} has $K*N$ rows and M columns and it is essentially sparse.

Thus, the problem of the lightning mapping consists of the direct and the inverse problems. The direct problem is solved by measurement of azimuthal histograms at different receiving stations of a network. The inverse problem is ill posed one with constrictions dictated by physical sense of desired nonnegative quantities of lightning intensity and can be solved by the regularized least squares method (see e.g. [5, 6]) by means of minimization of the next regularizing functional:

$$F(\vec{s},\beta) = \left(W\vec{s} - \vec{S}, W\vec{s} - \vec{S}\right) + \beta \cdot \left(\vec{s},\vec{s}\right), \quad (2)$$

where brackets $(\cdot,\cdot)$ denote scalar product, W is a system matrix, $\vec{S}$ is a vector representing a set of measured at different receiving points azimuthal distributions from equation (1). The norm of the unknown vector $\vec{s}$ is used as a stabilizer, and small positive regularization parameter β is determined by an empirical way.

3. Data acquisition

The experimental data used for this study were obtained from continuous measurements of VLF atmospherics azimuthal distributions performed on board the scientific vessel "Academician Vernadsky" moved around a south part of African continent in

February-April of 1991. A special measuring complex was developed and constructed for these measurements. The complex consists of three field component sensors: vertical electric (Er) and two horizontal orthogonal magnetic ones (Hx and Hy), band-pass filters (0.3-13 kHz), three-channel analog-to-digital converter, buffer memory device, personal computer, real-time software for preliminary processing and storing received data. Each atmospheric with amplitude exceeding a preestablished threshold level was digitised and transferred to the computer where direction to the source was determined. Averaged during half-our intervals azimuthal distributions with discrete of 5 degrees were stored to a hard disk for the further processing.

The method of the average Pointing vector in the time domain [7] used for direction finding let us to reach the registration rate of about 6000 pulses/hour. Atmospherics flow observed from the vessel board in the Indian ocean appeared concentrated within azimuthal sectors of about 30-40^{o} width covering the African and Asian global thunderstorm centres as can be seen from Fig.2.

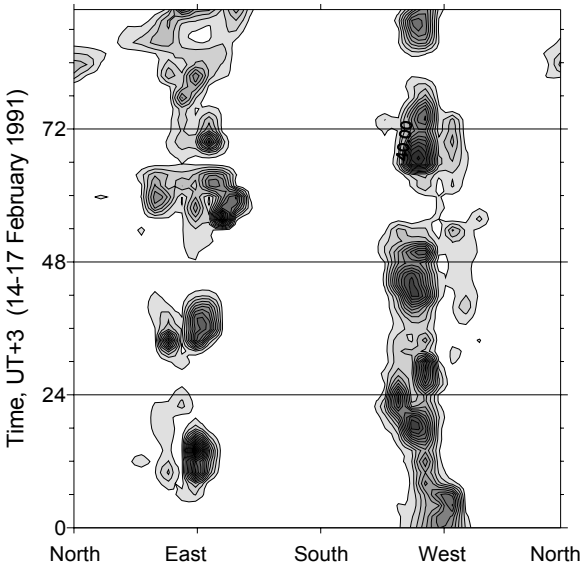

Fig.2

There were practically not observed VLF atmospherics arrived from north and south, and almost whole atmospherics flow concentrated near the west and east directions forming azimuthal distributions with characteristic shape of a 'butterfly'. In the vicinity of the Africa the structure these distributions became more complicated as is seen from Fig. 3, in which the average diurnal azimuthal distributions are plotted in the polar co-ordinate systems with centres corresponding to the daily median point of the vessel route.

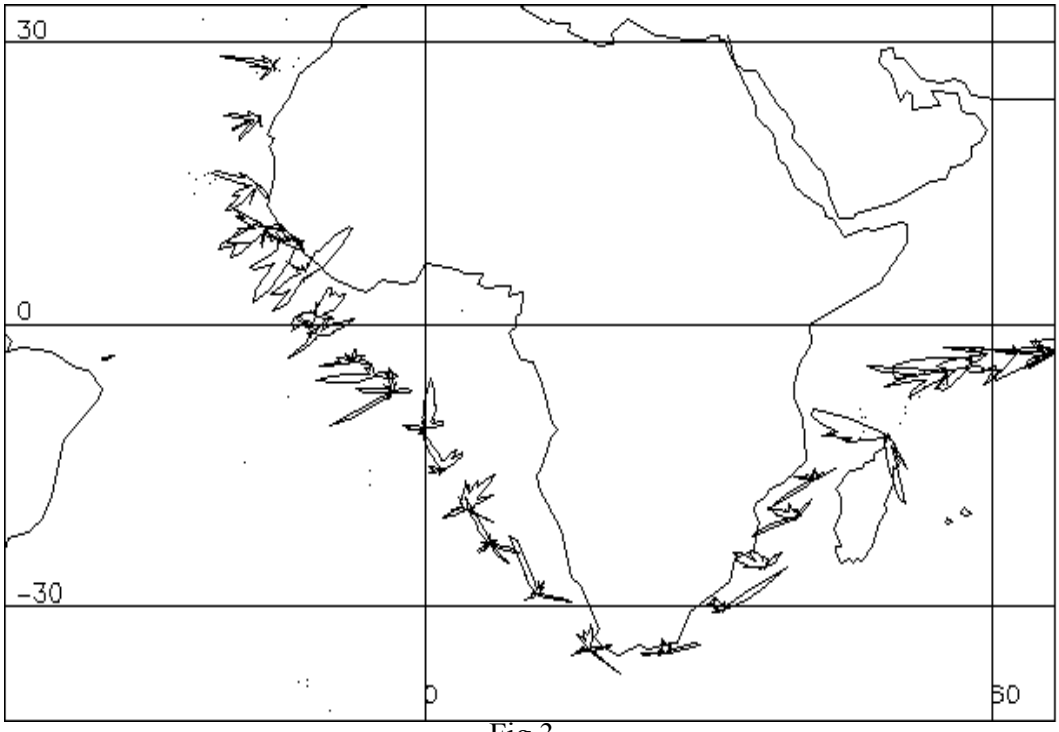

Fig.3

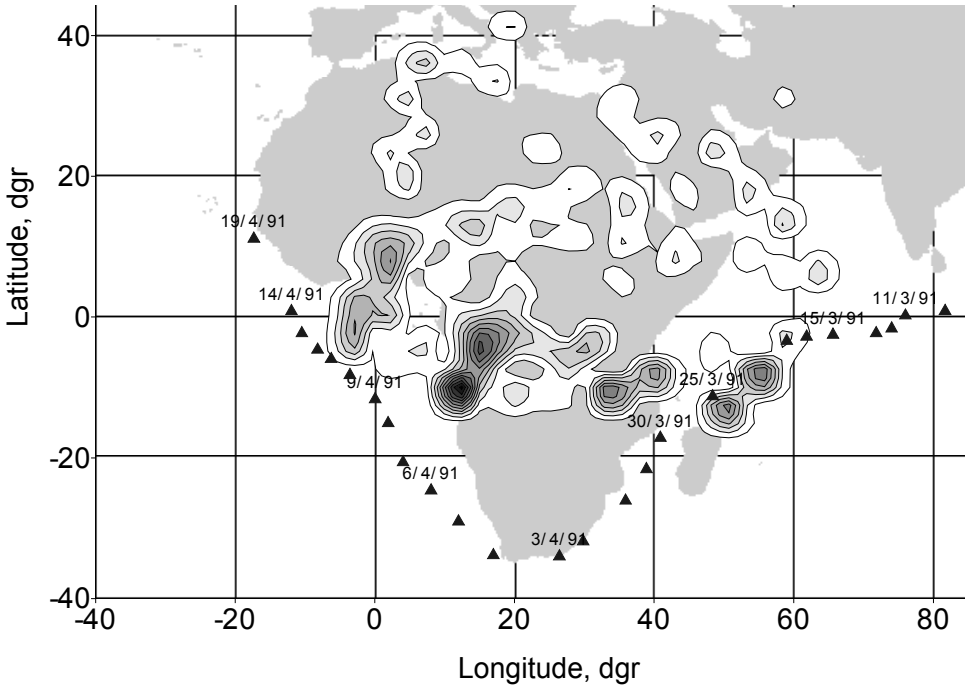

Fig.4

4. Results of tomographic reconstruction

We employ tomography reconstruction procedure based on multi-site measurements of VLF atmospherics azimuthal distributions. Virtual direction finders network was considered consisting of sites with co-ordinates determined as a median point of day part of the vessel's path. Two main problems are thought to appear in such a measurement scheme. As can be concluded from Fig.1 the main source of errors in reconstruction results is connected with existence of atmospherics outside of the area, covered by the network, which are being detected by only part of direction finders. This problem arises from limited detection range of LF-VLF receiving systems due to finite threshold level and relatively high attenuation for wave propagation within the earth-ionosphere waveguide.

Another important problem concerning with the analysis of the experimental data obtained at different points during the period exceeding one month is connected with considerable variability of the African sources from day to day as can be concluded from Fig.3.

To reduce these uncontrolled errors we considered azimuthal distributions corresponding to the periods of maximal sponding to the periods of maximal activity of the African world thunderstorm centre (14-16 UT) when the African sources dominate on others. We supposed also existence of stable active areas within the African continent during the observational period.

The results of reconstruction of the spatial structure of the African thunderstorms are represented as contour map in Fig.4. The daily average co-ordinates of the vessel are marked by solid triangles and partly by corresponding dates. These points we considered as virtual direction finder network. As we can see the resulting source distribution is noticeably structured and extended in the longitudinal direction. On the whole the African sources are shifted mainly to the south subequatorial latitudes that is inherent to the discussed spring period, when due to the seasonal drift, active areas start to move to the north direction. The four most intensive and relatively compact areas can be recognised in this figure. They tend to cover the basins of the great African rivers such as Niger and Congo, the islands of Madagascar and Seychelles. Considerable activity falls into the coastal part of the Guinea Bay. The sizes of these compact active areas are estimated as 1000-2000 km.

5. Conclusions

A technique for tomographic reconstruction of spatial distribution of lightning activity is proposed that allows to realize simplified in comparison with existing systems, lightning detection network which does not require strict synchronization between direction finders.

The technique was applied to experimental results of direction finding of VLF atmospherics obtained in Indian and Atlantic oceans during February-April 1991 on board of a scientific vessel to reveal a spatial structure of the African thunderstorm activity.

It was found that the lightning activity in Africa appear to be essentially structured and constituted by relatively compact active areas of maximal extension of 1000-2000 km that were predominantly concentrated over basins of the great rivers (Niger, Congo), Madagascar and Guinea Bay.

References

1. *Williams, E. R.* The Schumann Resonance: A global tropical thermometer. Science, 1992, 256, 1184-1187.

2. *Krider E.P., Noggle R.C., Pifer A.E, Vance D.L.* Lightning direction finding system for forest fire detection. Bull. Am. Meteorol. Soc., 1980, 61, 980-986.

3. *Hidayat S. and Ishii M.,* Spatial and temporal distribution of lightning activity around Java. Journ. Geophys. Res., 1998, 103, D12, 14001-14009.

4. *Shvets, A.V.* Worldwide lightning mapping with ELF tomography. 15th Int. Wroclaw Sympos. on EMC, June 27-30, 2000, part--2. 541-545.

5. *Lawson, C. L., R. J. Hanson,* Solving Least Squares Problems, Prentice Hall, ch.23, 1974, p.161.

6. *Tikhonov, A, and V. Arsenin,* Solutions of ill-posed problems, Wiley, New York, 1977.

7. *Nickolaenko A.P., Rafalsky V.A., Shvets A.V., and Hayakawa M.* A time domain direction finding technique for locating wide band atmospherics. Journ. Atmos. Electr., 1994, 14, 97-107.

Н. В. Киншт[1], Н. В. Силин[2], Ю. Б. Петропавловский[1]

[1]Институт автоматики и процессов управления ДВО РАН

[2]Дальневосточный государственный технический университет

МОНИТОРИНГ ЭЛЕКТРОМАГНИТНОГО ИЗЛУЧЕНИЯ ВЫСОКОВОЛЬТНОГО ОБОРУДОВАНИЯ

Abstract. This paper deals with characteristics of electromagnetic interference on outdoor high-voltage substation. The operation of the electric power equipment is always accompanied by its own intensive electromagnetic radiation with a wide frequency band. The electromagnetic signals, emitted by the high-voltage equipment can show serviceability or faults of this equipment. The spectrum voltages measured near the autotransformer 500 kV with and without defect are presented.

На территории открытых распределительных устройств (ОРУ) состав высоковольтного энергетического оборудования относительно стабилен.

Традиционно электрооборудование на ОРУ обслуживается по регламенту. Однако более экономный метод обслуживания – по состоянию. В настоящее время наблюдается высокая активность в разработке и применении новых методов диагностирования оборудования на основе использования современных информационно-измерительных комплексов.

Высокочастотное электромагнитное излучение (ЭМИ) генерируется высоковольтным энергетическим оборудованием в нормальном режиме работы. Обычно оно интерпретируется как неотъемлемая паразитная составляющая процесса использования электрической энергии, которая мешает приему и передаче радиосигналов. Источниками ЭМИ являются электрические разряды, возникающие как при нормальной работе оборудования, так и при деградации изоляции и других конструктивных элементов.

Подстанцию (ПС) в целом со всей схемой соединения оборудования можно рассматривать как сложную электрическую цепь, элементы которой электрически объединены процессом передачи энергии и общим полем электромагнитных излучений. В практике постановки задачи диагностирования до настоящего времени ПС обычно рассматриваются как совокупность единиц оборудования, которые по отдельности обладают свойствами индивидуального технического состояния (исправности либо неисправности) и которые надлежит индивидуально диагностировать. В то же время ПС может рассматриваться как совокупность связанных между собой элементов оборудования, являющихся источниками ЭМИ. Такими элементами могут быть силовые трансформаторы в целом или их вводы по отдельности, разъединители все или пофазно и т.д.

Элементы высоковольтного оборудования, являющиеся источниками ЭМИ, а также источники, расположенные вне ОРУ (радиостанции), формируют электромагнитную обстановку (ЭМО) на ПС, под которой понимают совокупность электромагнитных полей в рассматриваемой области.

Измерение спектра ЭМИ в широком диапазоне частот на территории ОРУ в различных точках наблюдения и дальнейшая его обработка позволяет выявить полезные с точки зрения диагностики сигналы. Анализ свойств этих сигналов с учетом физических свойств источников, пространственного расположения оборудования и схем соединения в конечном итоге позволит произвести оценку технического состояния высоковольтных установок.

Практически показано, что отдельные единицы высоковольтного оборудования имеют индивидуальные спектры ЭМИ.

Наличие ЧР в нормальном рабочем режиме существенно влияет на плотность сигналов и их амплитуду в отдельных частотных диапазонах. Эти диапазоны, как показывают наблюдения, являются характерными для отдельных видов оборудования.

Например, представленные на рис.1 спектры сигналов, измеренные вблизи группового силового автотрансформатора 500 кВ, имеют четко выраженные общие закономерности.

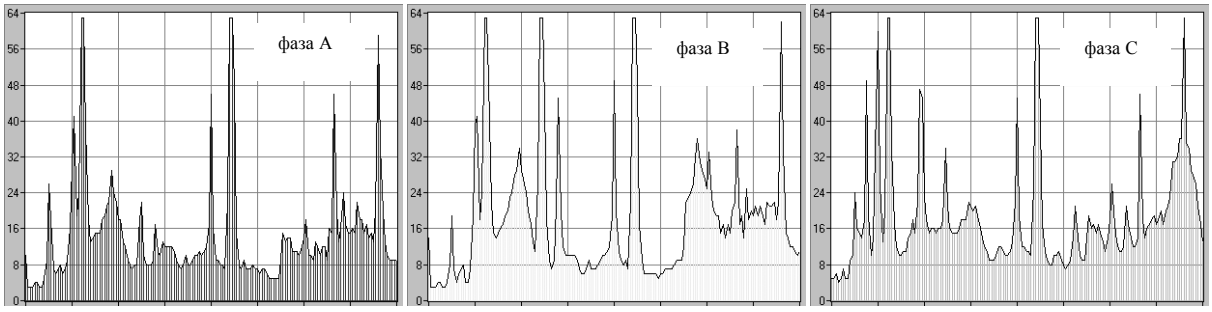

Рис. 1. Спектры сигналов вблизи группового силового автотрансформатора АТ-1.

Измерения проводились в широком диапазоне частот от 1 до 1000 МГц. Процессы, характерные для данного типа оборудования, позволяют обозначить поддиапазоны, связанные с излучением от ЧР.

Возникновение максимумов и минимумов в амплитудно-частотных характеристиках в отдельных диапазонах вполне может быть связано с наличием резонансных зон (до 1 МГц) и зоны вторичных резонансов (свыше 1 МГц) [1].

Наличие спектров сигналов, измеренных вблизи различных автотрансформаторов, позволяет выявить явное совпадение распределения сильных и слабых сигналов в некоторых информационных диапазонах.

Интерес представляют результаты измерений спектров излучений вблизи высоковольтного ввода 500 кВ автотранс-

форматора при обнаружении в нем дефекта.

Диэлектрические параметры изоляции ввода не превышали нормируемых значений и равны:

$$\text{tg}\,\delta_1 = 0{,}61;\ \text{tg}\,\delta_3 = 0{,}44;$$
$$C_1 = 638\ \text{пФ};\ C_3 = 45000\ \text{пФ}.$$

Однако данные хроматографического анализа растворенных газов указывали на превышение граничной концентрации, поэтому была дана рекомендация по замене ввода.

Критерий отношений концентраций определенных пар газов позволяет конкретизировать вид дефекта [2]. В основу этого критерия положена диагностическая схема публикации МЭК 599-78 с использованием отношений пар газов.

Анализ концентрации растворенных газов в дефектном вводе 500 кВ дал следующие результаты (% об):

CH_4 – 0,02744; C_2H_6 – 0,00651;
C_2H_4 – 0,00017; H_2 – 0,0204;
CO – 0,0234; CO_2 – 0,1102;
C_2H_2 – отсутствует;
$\Sigma\Sigma C_xH_y = 0{,}03412$.

Отношение $C_2H_2/C_2H_4 << 0{,}1$ в сочетании с отношением $CH_4/H_2 > 1$ надежно указывает на дефект термического характера. Отношение CO_2/CO меньше 10, что указывает на то, что тепловой и электрический дефект затрагивает твердую изоляцию.

Превышение концентраций газов предельного уровня вызывает развитие частичных разрядов, а следовательно и интенсивности электромагнитного излучения.

На рис. 2 изображены спектры сигналов вблизи бездефектного ввода 500 кВ (фаза А), а также вблизи ввода с вышеописанным дефектом (фаза В).

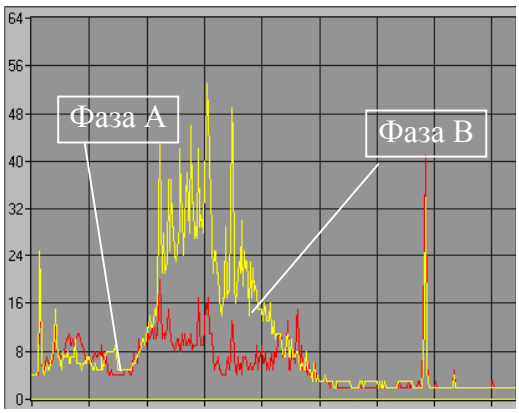

Рис. 2. Огибающие спектров вводов 500 кВ фазы А и фазы В автотрансформатора

Амплитуда сигналов дефектного ввода в отдельных поддиапазонах в 3 раза выше чем амплитуда сигналов бездефектного.

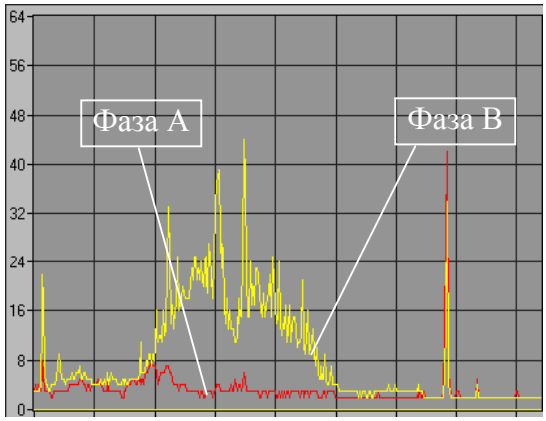

Рис. 3. Огибающие спектров вводов 220 кВ фазы А и фазы В автотрансформатора

На рис. 3 приведено наложение спектров сигналов от вводов 220 кВ, отличающихся друг от друга суммарным значением концентрации газов. Для фазы А суммарная концентрация ΣC_xH_y=0,00595, для фазы В ΣC_xH_y=0,01097.

Выводы:

1. Повышение суммарной концентрации газов в бумажно-масляной изоляции приводит к увеличению амплитуды сигналов ЭМИ.
2. Результаты измерения интенсивности ЭМИ вблизи высоковольтного оборудования могут быть использованы для

предварительной оценки технического состояния оборудования.

Литература

1. Левит А.Г., Поляков В.С., Шмерлинг Л.А. Из опыта измерений частичных разрядов силовых трансформаторов в эксплуатации. Из опыта работы высоковольтных сетей Ленэнерго. Л.: Энергоатомиздат, 1986.

2. Монастырский А.К. и др. Методы и средства оценки состояния маслонаполненного оборудования. Уч. пособие. ПЭИпк. С.-Петербург, 1996.

С. Ф. Чермошенцев, А. В. Шахов

Казанский государственный технический университет им. А. Н. Туполева

ПРИМЕНЕНИЕ МЕТОДА ГРАНИЧНЫХ ЭЛЕМЕНТОВ В ЗАДАЧЕ МОДЕЛИРОВАНИЯ РАСПРЕДЕЛЕНИЯ ПОТЕНЦИАЛОВ И ИМПУЛЬСНЫХ ПОМЕХ

Abstract. Pulse noise modelling in the ground circuits of the multilayer printed-circuit boards with the method of boundary elements is considered. The mathematical model and it's software implementation are developed. The results of the pulse noise analysis in test problem are presented.

В настоящее время применение субнаносекундных интегральных схем и многослойных печатных плат (МПП) в электронных средствах показало, что задача обеспечения электромагнитной совместимости и помехоустойчивости электронных средств является одной из важнейших. При этом возрастают требования к помехоустойчивости интегральных схем, особенно по отношению к импульсным помехам по цепям питания и заземления [1, 2].

Цель данной работы - разработка модели для анализа импульсных помех в цепях заземления МПП и её программной реализации.

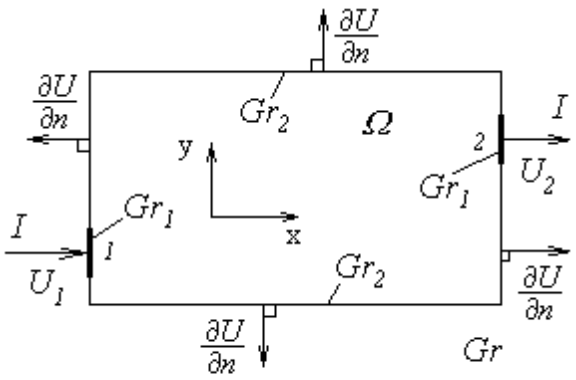

Рис. 1. Модель шины земли МПП

В работе моделируются импульсные помехи в проводящем слое земли МПП (рис. 1).

В точках 1 и 2 подсоединены выводы земли двух интегральных схем, в точке 1 ток втекает, а в точке 2 вытекает. Для моделирования используется уравнение [3, 4, 5] вида:

$$\nabla^2 U(x,y,t) = (RC + L\Theta)\cdot\frac{\partial U(x,y,t)}{\partial t} \quad (1)$$

где U –потенциал в слое земли МПП; R, C, L, Θ –соответственно сопротивление, ёмкость, индуктивность и проводимость единичного участка слоя земли; при соответствующих зависящих от времени граничных условиях следующих двух типов:

$\partial U/\partial n = 0,\ U = U_0$ на Gr_1 и

$\partial U/\partial n = q_0, U = 0$ на Gr_2 в момент времени 0 и

$\partial U/\partial n = 0,\ U = U_t$ на Gr_1 и

$\partial U/\partial n = q_t, U = 0$ на Gr_2 в момент времени t

где Gr_1 и Gr_2 –части границы, где задается то или иное условие. Полная граница рассматриваемой области равна

$Gr = Gr_1 \cup Gr_2$. Пусть заданы некоторые начальные значения в области исследования Ω в момент времени $t = 0$: $U(0) = 0$.

Для решения задачи применяется метод граничных элементов (МГЭ) [3, 4]. Суть метода состоит в преобразовании дифференциального уравнения в частных производных, описывающего поведение неизвестной функции внутри и на границе области, в интегральное уравнение, определяющее только граничные значения, и затем отыскании численного решения этого уравнения. Если требуется найти значения потенциала во внутренних точках области, то их можно вычислить, используя известные решения на границе. Поскольку все обусловленные численными расчетами приближения связаны только с границей, получаемая система уравнений имеет меньшую размерность по сравнению с размерностью исходной системы дифференциальных уравнений.

Граница слоя земли Gr при использовании МГЭ разбивается на N сегментов, или граничных элементов, из которых часть элементов относятся к части Gr_1 границы, а часть элементов - к Gr_2.

Точки, в которых рассматриваются неизвестные величины, называются узлами; они находятся в середине каждого постоянного элемента. Значения функций U и $Q=\partial U/\partial n$ предполагаются постоянными для каждого элемента и равными их значениям во внутреннем узле элемента. Для каждого элемента известна одна из двух функций (U или Q). Граничное интегральное уравнение можно получить с помощью метода взвешенных остатков [3, 4]:

$$s \cdot U_i + \frac{1}{RC + L\Theta} \cdot \int_{Gr} U \cdot Q^* dGr = \\ = \frac{1}{RC + L\Theta} \cdot \int_{Gr} Q \cdot U^* dGr + \frac{1}{\Delta t} \cdot \int_{\Omega} U_0 \cdot U^* d\Omega \qquad (3)$$

где

$$U^* = \frac{RC + L\Theta}{2\pi} \cdot \ln \frac{1}{r} - \frac{RC + L\Theta}{4\pi} \cdot \ln \frac{RC + L\Theta}{\Delta t} \qquad (4)$$

– фундаментальное решение для уравнения (1);

$$Q^* = \frac{\partial U^*}{\partial n} = \frac{RC + L\Theta}{2\pi} \cdot (x - x_i) \cdot \cos(n, ox) + \\ + \frac{RC + L\Theta}{2\pi} \cdot (y - y_i) \cdot \cos(n, oy)$$

– производная функции U^* по нормали;

r – расстояние между двумя точками на границе;

Коэффициент $s = 1$ во внутренних точках, $s = 1/2$ на границе; cos (n, ox) и cos (n, oy) –направляющие косинусы нормали, где (n, ox) и (n, oy) –углы между нормалью и осями координат.

Соотношение (3) записано для отдельного i-го узла. Это отношение связывает значение функции U в точке i со значениями функций Q и U на границе Gr.

В выражение (3) входит поверхностный интеграл, но он не вводит никаких дополнительных внутренних неизвестных. Для его нахождения область Ω разбивается на ряд ячеек, или внутренних треугольных элементов, необходимых для проведения процедуры численного интегрирования.

Соотношение (3) в дискретном случае можно записать для точки i (не задавая конкретных граничных условий), и вынося функции U_j и Q_j из-под знака интеграла (поскольку они предполагаются постоянными по длине элемента), получаем:

$$s \cdot U_i + \frac{1}{RC + L\Theta} \cdot \sum_{j=1}^{N} \left(\int_{Gr_j} Q^* dGr \right) \cdot U_j = \\ = \frac{1}{RC + L\Theta} \cdot \sum_{j=1}^{N} \left(\int_{Gr_j} U^* dGr \right) \cdot Q_j + \\ + \frac{1}{\Delta t} \cdot \sum_{k=1}^{M} \left(\int_{Gr_k} U_0 \cdot U^* dGr \right) \qquad (6)$$

Интеграл $\int_{Gr_j} Q^* dGr$ устанавливает связь i-го узла с j-м сегментом, по которому проводится интегрирование, и обозначается H_{ij}. Аналогично интегралы $\int_{Gr_j} U^* dGr$ в правой части этого соотношения имеют вид и будут обозначаться через G_{ij}. Эти интегралы можно вычислить одним из численных методов. Тогда соотношение (6) примет вид:

$$s \cdot U_i + \frac{1}{RC + L\Theta} \cdot \sum_{j=1}^{N} \hat{H}_{ij} \cdot U_j = \frac{1}{RC + L\Theta} \cdot \sum_{j=1}^{N} G_{ij} \cdot Q_j + \frac{1}{\Delta t} \cdot \sum_{k=1}^{M} \left(\int_{Gr_k} U_0 \cdot U^* dGr \right) \quad (7)$$

Выражение (7) можно записать для каждого i-го рассматриваемого узла. Вводится следующее обозначение:

$$H_{ij} = \begin{cases} \hat{H}_{ij} & при \quad i \neq j \\ \hat{H}_{ij} + \frac{1}{2} & при \quad i = j \end{cases}$$

Тогда (7) может быть переписано в виде:

$$B_i + \sum_{j=1}^{N} H_{ij} U_j = \sum_{j=1}^{N} G_{ij} Q_j ,$$

где $\hat{H}_{ij} = \frac{1}{RC + L\Theta} \int_{Gr_i} Q^* dGr$;

$$G_{ij} = \frac{1}{RC + L\Theta} \int_{Gr_i} U^* dGr ;$$

$$B_i = \frac{1}{\Delta t} \int_{\Omega} U_0 U^*_{\Delta t} d\Omega = \frac{1}{\Delta t} \sum_{k=1}^{M} \left(\int_{Gr_k} U_0 U^*_{\Delta t} dGr \right);$$

Интегралы H_{ij} и G_{ij} можно вычислить, используя простые квадратурные формулы Гаусса. Метод квадратур Гаусса был реализован в программе MGE [6] в виде одной из функций библиотеки.

Полная система NxN уравнений для N узлов может быть представлена в матричной форме:

$$\mathbf{HU} = \mathbf{GQ} + \mathbf{B} \quad (8)$$

Если на границе Gr известны N_1 значений функции U и N_2 значений Q, то в уравнении (8) будет содержаться только N неизвестных, которые могут быть выражены через исходные значения, и эту систему следует преобразовать, с тем чтобы её порядок был уменьшен и равен числу рассматриваемых неизвестных. Уравнение (8) можно преобразовать путем переноса всех неизвестных в левую часть, тогда в правой части остается вектор, получаемый умножением элементов матрицы на известные значения потенциала и потока, что дает:

$$\mathbf{AX} = \mathbf{F} \quad (9)$$

где **X** -вектор, компонентами которого являются неизвестные значения функций U и Q. Вектор **F** включает вектор **B**. Матрица **A** является полностью заполненной матрицей порядка N. Система линейных алгебраических уравнений (9) может быть решена методом Гаусса.

Данный метод реализован в программе MGE также в виде одной из функций библиотеки. Решив уравнение (9), можно найти значения U и Q на границе. Поскольку значения U и Q известны на всей границе, можно вычислить значения и в произвольных внутренних точках, учтя вклад членов, содержащих функцию B с помощью соотношения (3).

Уравнение (1) включает функцию времени. Один из путей его решения состоит в использовании шаговой по времени процедуры, когда задача решается для каждого временного интервала, и значения, полученные на каждом предыдущем шаге, используются как псевдоначальные условия на последующем шаге, что и реализовано в программе MGE.

Программа MGE была разработана на языке программирования C++ и позволяет рассчитать неизвестные значения потенциалов и импульсных помех как на грани-

це, так и внутри области исследования при источниках, расположеных на границе. Размер программы 860 Кб.

Алгоритм программы представлен на рис. 2.

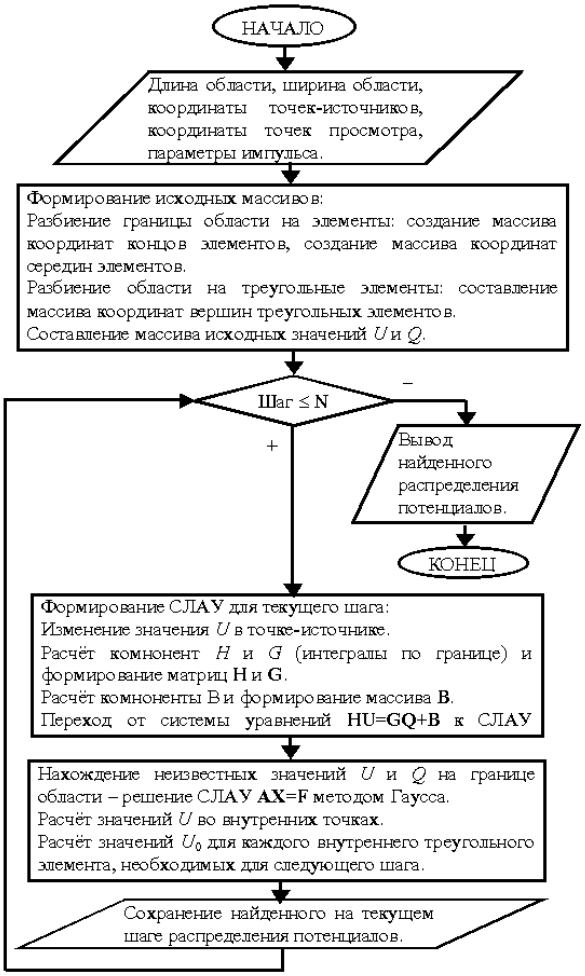

Рис.2. Алгоритм программы MGE

Входные данные программы MGE: 1) размеры области исследования (длина, ширина); 2) номера граничных элементов, на которых расположены источники; 3) координаты точек наблюдения (точки, в которых требуется получить результат). Выходные данные: значения потенциалов и импульсных помех в точках наблюдения. Выходные данные представляются в виде таблицы и осциллограмм.

В качестве примера моделирования была взята шина земли МПП размером 120x100 мм (рис. 3) с параметрами R=10^{-3}Ом, C=15.6Пф, L=9.6нГн, Θ=10^{-15} См.

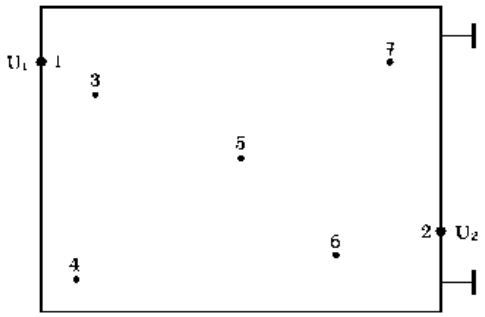

Рис.3. Объект моделирования: шина земли МПП

В точках 1 и 2 подсоединены выводы земли двух интегральных схем. В точке 1

втекает трапецевидный импульс с фронтом 1 нс, амплитудой 1 В и длительностью 10 нс. Внутренние точки 3, 4, 5, 6, 7 выбраны точками просмотра. Так как при использовании метода граничных элементов нужно задавать на каждом элементе значения либо U, либо $\partial U/\partial n$, в остальных точках границы задаём $\partial U/\partial n$=0.

Координаты точек 1 и 2 по x, y (мм.): 1: 0, 80; 2: 120, 30. Координаты точек наблюдения по x, y (мм.): 3: 20, 70; 4: 10, 10; 5: 70, 50; 6: 80, 20; 7: 110, 80.

Максимальные значения импульсных помех

Таблица

Число элементов	Точки наблюдения				
	3	4	5	6	7
880	0,7554	0,5502	0,3826	0,2005	0,0253
440	0,7554	0,5500	0,3826	0,2000	0,0251
220	0,7552	0,5495	0,3821	0,1992	0,0248
110	0,7531	0,5450	0,3784	0,1990	0,0243

В таблице приведены максимальные значения импульсных помех во внутренних точках наблюдения для различного количества взятых элементов по границе.

Таким образом, предложенная математическая модель для анализа импульсных помех (потенциалов) на шинах земли МПП и её программная реализация позволяют оценивать уровни данных помех в различных конструктивных исполнениях МПП, отличающихся видом слоя земли (сплошная, сетка и решётка) и величинами электрических параметров *R, C, L и Θ*.

Литература

1. Барнс Дж. Электронное конструирование: Методы борьбы с помехами: Пер. с англ. –М.: Мир, 1990. – 238 с.
2. Шваб А. Электромагнитная совместимость / Пер. с нем. В. Д. Мазина и С. А. Спектора, 2-е изд., перераб. и доп.; Под ред. И. П. Кужекина. – М.: Энергоатомиздат, 1998.- 480 с.
3. Бреббия К., Теллес Ж., Вроубел Л. Методы граничных элементов.- М.: Мир, 1987. – 524 с.
4. Бреббия К., Уокер С. Применение метода граничных элементов в технике.- М.: Мир, 1982. – 248 с.
5. Деньдобренько Б. Н., Малика А. С. Автоматизация конструирования РЭА.- М.: Высш. школа, 1980. – 384 с.
6. Чермошенцев С. Ф., Шахов А. В. Моделирование импульсных помех на шинах земли многослойных печатных плат методом граничных элементов //Электромагнитная совместимость технических средств и биологических объектов: Сб. докл. VI Рос. науч.–техн. конф. –С.–Пб., 2000. –С. 255-259.